AN ABSTRACT OF THE THESIS OF

Kyle J. Hoover for the degree of Master of Science in Nuclear Engineering presented on December 14, 2016.

Title: SMR Full-Power Scaling Analysis and Numerical Simulation for Nuclear Hybrid Energy System Testing

Abstract approved: _____

Qiao Wu

A scaling analysis of the Oregon State University (OSU) - Multi-Application Small Light Water Reactor (MASLWR) system has been developed, and an existing RELAP5-3D model of the facility was improved. The purpose of this study is to support the research of hybrid energy systems, being led by Idaho National Laboratory (INL). Hybrid energy systems have recently become a point of interest for their ability to combine nuclear and non-nuclear clean power generation, while also providing energy storage and industrial production capabilities. Hybrid Energy Systems could well utilize small modular reactors (SMRs). For this study, the specific requirement is a RELAP5-3D model of the NuScale design. The OSU-MASLWR system modeled an older version of the NuScale design, so the RELAP model is based on that facility. However, MASLWR was not scaled for the types of testing that INL requires, so a new set of scaling parameters was developed. The RELAP model was benchmarked against IAEA data from an International Collaborative Standard Problem study performed at MASLWR in 2010. This work shows that the RELAP model agrees well with test data, and is therefore suitable for simulating the performance of the MASLWR system for nuclear hybrid energy system testing.

©Copyright by Kyle J. Hoover
December 14, 2016
All Rights Reserved

SMR Full-Power Scaling Analysis and Numerical Simulation for Nuclear Hybrid Energy System Testing

by

Kyle J. Hoover

A THESIS

submitted to

Oregon State University

in partial fulfillment of
the requirements for the
degree of

Master of Science

Presented December 14, 2016
Commencement June 2017

Master of Science thesis of Kyle J. Hoover presented on December 14, 2016.

APPROVED:

Major Professor, representing Nuclear Engineering

Head of the School of Nuclear Science and Engineering

Dean of the Graduate School

I understand that my thesis will become part of the permanent collection of Oregon State University libraries. My signature below authorizes release of my thesis to any reader upon request.

Kyle J. Hoover, Author

ACKNOWLEDGEMENTS

Although I worked very hard on my graduate degree in my own right, I certainly did not do it alone. I would like to thank Dr. Qiao Wu for his support as my advisor, and for the opportunities he afforded me through the MASLWR program. To my research group, I offer my thanks for the advice I was given in meetings, and for the mutual respect that we kept between each other to drive us to achieve. A very special thank you to Dr. Brian Woods, Ben Bristol, Claudio Delfino, and Dr. Jeffrey Luitjens for their support and advice regarding RELAP5-3D, and computer modeling in general. Another special thank you to Chris Thompson for always helping me keep the various softwares that I needed up and running. My parents, Kim and Jim, as well as the rest of my family were unfailing in their support of my pursuit of my Master's Degree. I'm thankful to my friends, both from my work at the radiation center, and in my personal life, that never failed to bring my spirits up. Without all of you, I truly believe this would not have been possible.

TABLE OF CONTENTS

TABLE OF CONTENTS (Continued)

LIST OF FIGURES

LIST OF FIGURES (Continued)

LIST OF TABLES

Chapter 1: Introduction

Renewable energy systems are becoming more and more common all over the world. Among their many benefits, renewables also have a considerable drawback: their power output is not dispatchable. Due to their variable nature, hybrid energy systems have been proposed to help meet grid demand. By combining renewable energy sources with a nuclear power generating station, electrical output can be varied to achieve this goal. Energy sinks are also necessary in the process, to allow for variation in the nuclear system's steam output to the turbines. Excess steam can be directed to process heat, water desalination, and thermal storage. These opportunities to better integrate clean energy into the economic structure of the grid require research in the area of controls, optimization, and energy storage. [3][11]

1.1 Hybrid Energy Technology

The motivations behind a hybrid energy plant include reduced greenhouse gas emissions, and increased energy efficiency and reliability. These motivations are driven primarily by the Department of Energy's (DOE) goals for the US energy structure in the coming decades [12]. A hybrid energy plant is, in theory, a combination of a nuclear power generating station for baseload power supply, a renewable energy production facility (e.g. wind or solar), and energy storage (thermal and/or electrical), and process heat facilities [1]. The combined energy system meets the needs of the electrical grid, either through load following of the nuclear reactor, or diversion of steam from the secondary side to the thermal storage and process heat facilities. An example of this kind of system is presented in Figure 1.1. The nuclear reactor's secondary side provides steam to an intermediate heat exchanger,

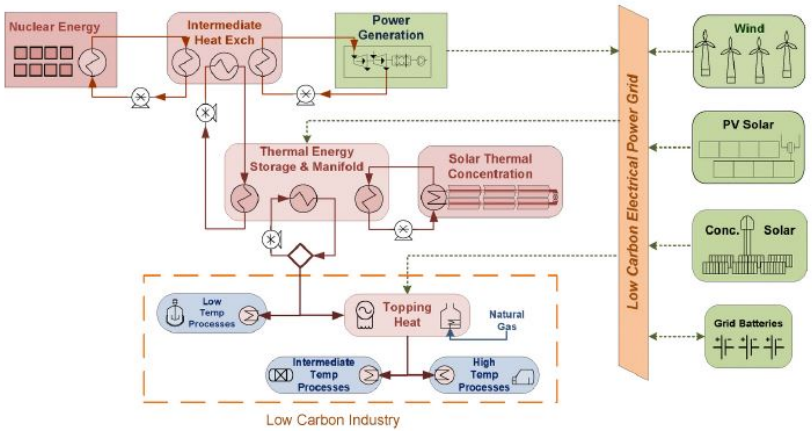

Figure 1.1: Hybrid energy plant example, utilizing wind power and auxiliary thermal processes [1]

which varies the thermal load between the turbine and the thermal energy storage buffer. Heat is then transferred to other processes where appropriate. This operating strategy allows grid demand to be met, without wasting excess generation. The problem with this strategy is that everything from seasonal to daily variations in electrical power demand dictate that the nuclear plant must run below maximum capacity for considerable amounts of time in a given year, necessitating advanced control algorithms to safely operate the reactor and to properly meet demand. Research is required in this area to raise the technology readiness level of coupling such systems.

1.2 Small Modular Reactors

Small modular reactors (SMRs) are a new development in the nuclear industry. They largely utilize existing technology of light water reactors (LWRs) in a more compact and modular manner, and fall into the "generation 3+" category. Of particular interest to this study is the NuScale Power SMR design. Figure 1.2 presents the conceptual design of a single nuclear power module. The proposed

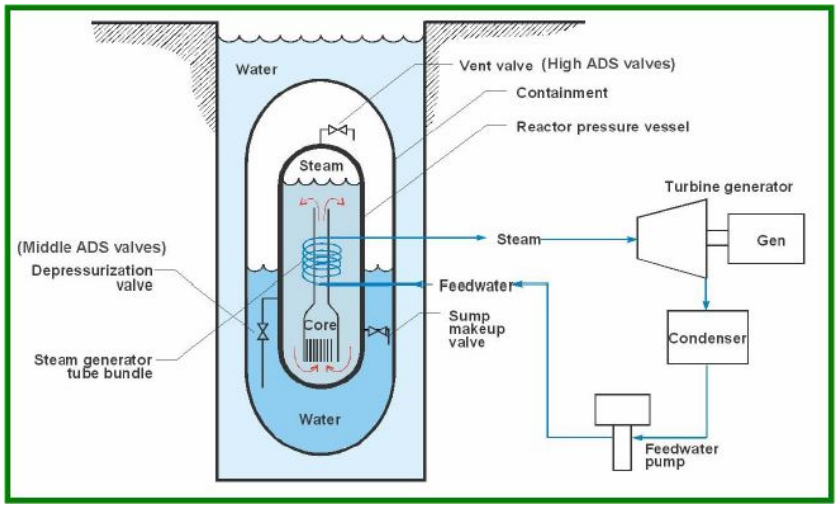

Figure 1.2: NuScale module conceptual design [2]

plant would house up to 12 of these modules in a single cooling pool. The primary circuit flow is driven entirely by natural circulation with the nuclear core as the heat source and a helical coil steam generator as the heat sink. The pressurizer is integral to the reactor pressure vessel and allows pressure communication through a baffle plate between the pressurizer region and the primary circuit region. In the event of an accident, the vent valves at the top of the reactor vessel open to allow coolant to flow into the containment vessel, which releases heat to the cooling pool that the reactor module sits in. Once the pressure in the containment vessel has built up to the point that fluid can be forced from the containment vessel back into the reactor vessel, the sump makeup valves then open to allow coolant to flow back into the core. This forms a natural circulation loop between the core and the containment wall which cools the core adequately after a SCRAM. The entire process is driven by physics and control system trips, requiring no operator input.

This type of SMR design is desirable for hybrid energy applications because there are 12 modules operating at any given time, and it is feasible to only need to load follow with one module as opposed to the entire core of a standard LWR, depending on the load demand. The implied safety advantages are that if compli-

cations arise with the load following module, only 1/12 of the total thermal power must be attended to with emergency procedures while the other 11/12 of the power can be shut down normally if necessary. Furthermore, six of the reactor modules are located in a common cooling pool (two cooling pools per plant), which provides the ultimate heat sink in accident conditions.

1.3 Objectives

This thesis contributes to the development of methods for load following activities for hybrid energy applications. Idaho National Laboratory has assembled a team of institutions to investigate applications of load following to hybrid energy plants, including North Carolina State University, Massachusetts Institute of Technology, Ohio State University, the University of New Mexico, and Oregon State University. Oregon State's role in this project is to supply data from the International Collaborative Standard Problem (ICSP) testing that was performed at the OSU Multi-Application Small Light Water Reactor (MASLWR) test facility in 2010, and to provide a RELAP5-3D model for running simulations to help validate models being developed by the other institutions. In order for the data to be applicable to full power testing, however, an alternate set of scaling parameters for the MASLWR facility must be developed. This is discussed further in chapter 4. This thesis' main objectives include:

- Develop full power scaling parameters for the MASLWR facility
- Modify/improve and benchmark RELAP5-3D model of the MASLWR facility

Chapter 2: Literature Review

This chapter provides a review of relevant literature for the subjects of this study shall be performed. Relevant subjects include the fields of thermal hydraulic modeling (via RELAP5-3D), system scaling, hybrid energy, and load following.

2.1 Load Following and Hybrid Energy Technology

Given that research in nuclear hybrid energy technology is the motivation for this study, it is prudent to develop an understanding of the general state of the industry in this regard. Initial motivation for the study of hybrid energy technologies derives from the economics of the energy industry. Forsberg states in his paper "Hybrid systems to address seasonal mismatches between electricity production and demand in nuclear renewable electrical grids" that there are massive motivations to move away from fossil fuels; necessitating the use of nuclear and renewable energies. Renewable technologies cannot, however, strictly control energy output. The demand from the electrical grid load also varies from an hourly to seasonal scale, so operations with renewables are challenging [3].

Studies have been performed to develop control strategies for load following with nuclear plants, but this is very technically challenging. Disruption of axial flux distributions that often result from load following give rise to xenon oscillations [13]. Effects like these necessitate complicated predictive controllers, and/or very adept operators for the plant to operate safely and economically. In the United States, load following is typically achieved by varying the chemical shim injection, though power adjustment with control rods is also used [14]. These types of methods have been successfully implemented in France and Germany, where load

following activities are anticipated to be commonplace. In these countries, the regulatory environment is structured such that load following is accounted for in proper operation and design validation [15]. These regulatory and design considerations are not common in the United States, and would need to be implemented before widespread use of load following practices. C

Hybrid energy technologies face similar challenges. Some of the closest existing examples of hybrid energy plants are cogeneration plants. A cogeneration plant at the University of Connecticut provides the campus with electricity, steam, and chilled water. These three processes have different demands based on the season; thus, the plant has three main operating modes. Each of these modes makes up excess demand depending on the season, i.e. extra steam in the winter months, and extra chilled water in the summer months [16]. Recalling figure 1.1, a hybrid energy plant would be equipped with similar processes and capabilities. The thermal storage strategies allow for energy to be stored in times of over-production, and then used in times of under-production [3]. This improves upon the cogeneration strategy, which simply generates more power to make up for losses.

Hybrid systems would utilize entirely clean energy. Since renewable energy sources like wind and solar experience such wide variations in production, seasonal and daily energy storage strategies are a must for long-term market viability if their use is not coordinated with baseload power supply. Figure 2.1 shows an example of the weekly averaged production of wind, solar, and nuclear energies in California in 2005. The plot shows that production from the renewable sources wildly mismatched demand at nearly all points during the year. Although the plots are from different years, Figure 2.2 shows the effect this can have on the electricity market. Prices become highly volatile and even drop to negative values [3]. Some more recent studies conducted by INL have shown similar results on a weekly scale, and are presented in figures 2.3 and 2.4 for wind and solar power respectively. The tenet of hybrid systems is that the excess energy is always used, such that there is no excess generation, resulting in stabilizing electricity prices.

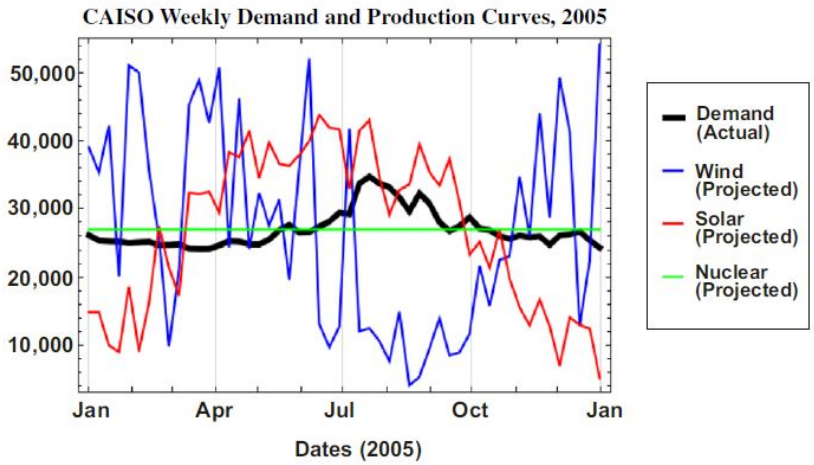

Figure 2.1: Idealized California electricity demand and production (MWe) for 2005 [3]

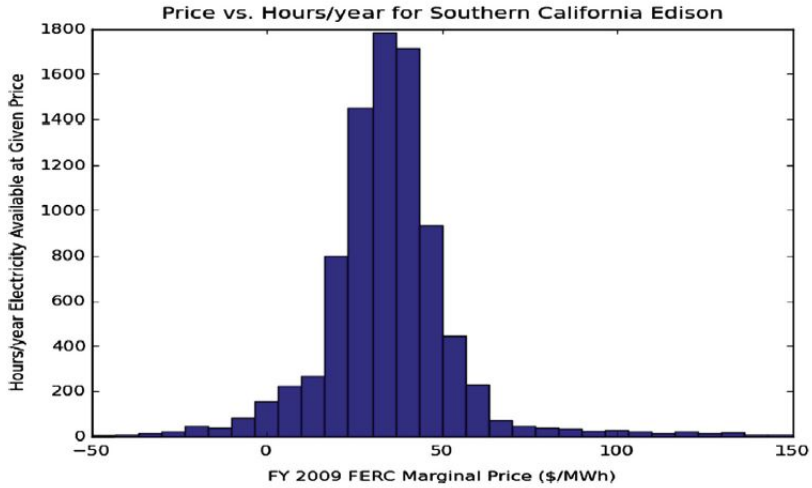

Figure 2.2: Electricity prices for southern California during 2009 [3]

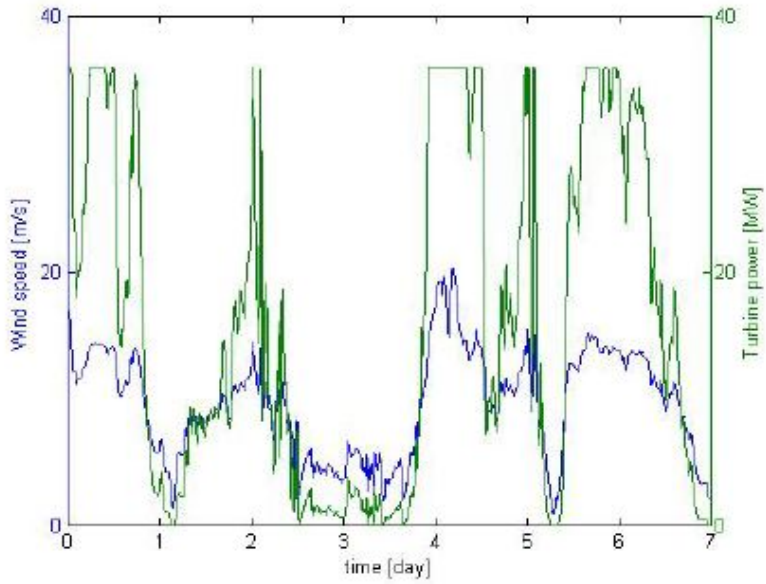

Figure 2.3: Wind speed and turbine power for a period of seven days in Texas [4]

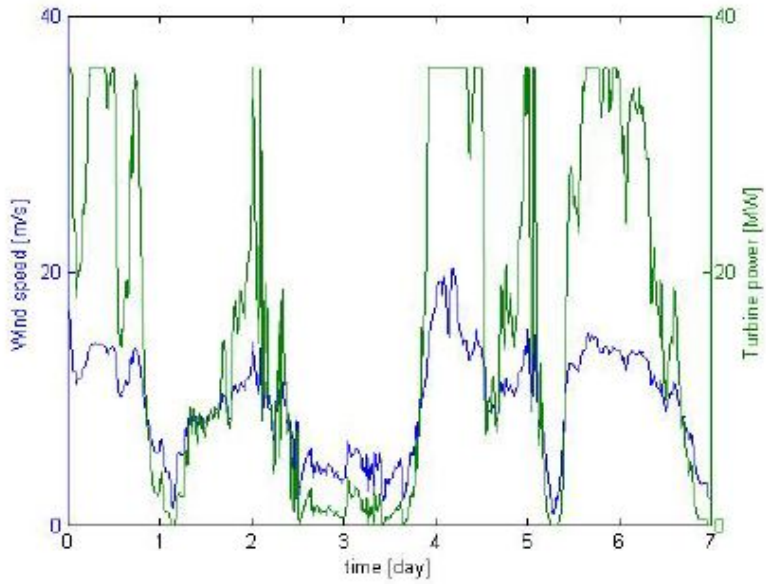

Figure 2.4: Solar irradiation and PV solar power for a period of seven days in Arizona [4]

Recalling the discussion of section 1.1, the hybrid system would utilize excess thermal energy to supply industrial processes, or is routed to a thermal storage device. The storage device stores thermal energy in times of over-production for use in times of under-production. Thermal storage devices comprise one of many options, however. Beyond process heat for industrial processes, there is great interest in hydrogen production using hybrid plants. Small-scale hydrogen production is less economically viable than large-scale production. Given the wealth of applications for hydrogen power, production on an economic scale could prove extremely useful in meeting future demands, and hybrid plants [17].

2.2 RELAP5-3D

The Reactor Excursion and Leak Analysis Program (RELAP) is a well known thermal hydraulic modeling software package developed by Idaho National Laboratory. Sponsored by various organizations such as the U.S. Department of Energy, and the U.S. Nuclear Regulatory Commission, the code is intended to model system level transients in light water reactors. Such transients often include loss of coolant accidents, loss of feedwater, loss of offsite power, station blackout, and turbine trips [18]. The specific version of the code used in this study is RELAP5-3D v4.0.

RELAP5-3D is a 1-dimensional system code based on a semi-implicit finite-difference scheme using the two-fluid model. The two-fluid equations are formulated in terms of volume and time-averaged parameters. This requires that all phenomena that depend upon transverse gradients in the flow (such as friction and heat transfer) are defined via empirical transfer coefficient formulations that utilize the bulk fluid conditions as inputs [18]. Code structures are broken up into two main types of components: hydrodynamic components and heat structures. Hydrodynamic components store information on the system's working fluid, i.e. the temperature, pressure, fluid properties, void fraction, flow rates, and other such terms. The heat structures typically represent solid physical structures such as the tubes of a heat exchanger or the wall of the vessel. The hydrodynamic volumes and heat structures interact to simulate heat transfer between hydrodynamic volumes or as constant thermal boundary conditions.

Pursuant to the goals of this study, it is important to realize certain limitations of RELAP5-3D. First RELAP5-3D v4.0 is unable to properly model a helical coil steam generator. Recall from the previous paragraph that RELAP5-3D relies on empirical correlations for its numerical scheme. RELAP5-3D v4.0 does not possess correlations for helical coil heat exchangers, and thus cannot explicitly model the MASLWR steam generator. Because the momentum field equation for RELAP5-3D is invariant in transverse directions [18], the mixing effects of a helical tube will

not be captured. This is discussed further in section 5.2.2. Further, while RELAP5-3D has shown satisfactory results in some studies for parallel flow prediction in two-tube geometries, its abilities are in question for more complicated geometries [19]. Given that MASLWR's steam generator is made up of 13 separate tubes with common inlet and outlet headers, accurate simulation of each tube individually is not practical for the scope of this study. Thus, simplifications made to the model are detailed in section 5.2.2.

This study intends to use RELAP5-3D to model processes dominated by natural circulation. Hence, it must be verified that RELAP5-3D is reasonably capable of doing so. Various studies have been performed to this end. Reference [20] shows that an older version of RELAP5 (RELAP5/MOD2) was compared against a natural circulation experiment, and showed adequate qualitative agreement, although a quantitative approach could not be taken. It has been found in reference [21] that RELAP5's ability to model various natural circulation flow effects depends significantly on the nodalization scheme used, but not the specific node sizes relative to the facility dimensions. It is noted in reference [21] that many of the disagreements occur from flow instabilities that arise during natural circulation. Furthermore, reference [22] notes that while all codes involved in its study (including RELAP5) had some challenges in accurately simulating natural circulation flow rates, it is shown that the single phase natural circulation flow was adequately predicted by RELAP5. So, although results are thus far inconclusive, RELAP5 is generally considered to capture single phase natural circulation flows adequately, which is within the scope of this study.

2.3 Scaling

Scaled test facilities have been utilized more and more in the nuclear industry over the past 20 to 30 years. Whether contributing to design basis accident analysis for new types of reactors or being used to develop new correlations and other

studies, scaling is used for a wide variety of tasks. In the context of this study, scaling is used on the integral system test facility, MASLWR (description in chapter 3). The specific method used herein is the Hierarchical Two-Tiered Scaling (H2TSg) method. One of the first applications of this methodology was on the OSU Advanced Plant Experiment (APEX) facility and has since been applied to the MASLWR system, among others. The H2TS methodology is used in this study because the original MASLWR scaling was performed with H2TS and is still in use today. Since the original scaling is needed to develop the new scaling parameters, H2TS must be used.

The development of the H2TS method is described in detail in reference [5]. The method was originally developed to help support the goals of the Severe Accident Research Program (SARP) which was formed by the Nuclear Regulatory Commission (NRC). The plan's development was based on the Integrated Structure for Technical Issue Resolution (ISTIR), which is presented in figure 2.5. Note that SASM and CSAU stand for Severe Accident Scaling Methodology, and Code Scaling, Applicability, and Uncertainty methodology, respectively. The interested reader is encouraged to read reference [5] for the full description, but the overall H2TS method is essentially described by figure 2.6.

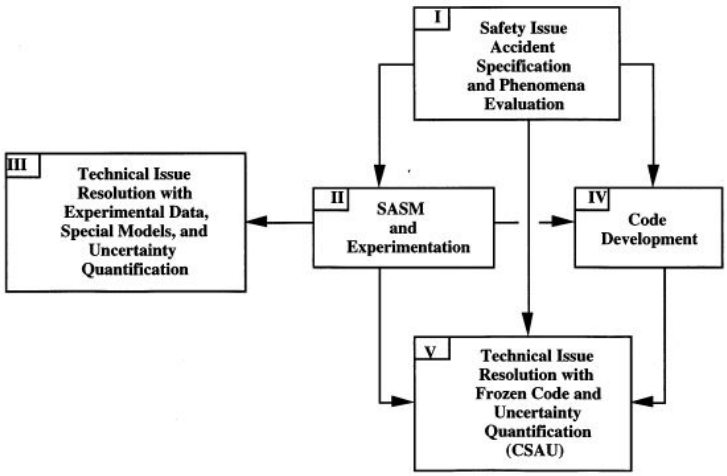

Figure 2.5: Integrated Structure for Technical Issue Resolution [5]

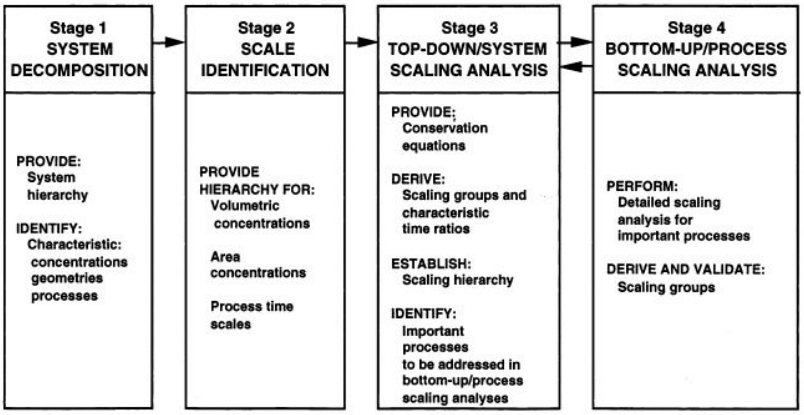

Figure 2.6: Stages of the H2TS method [5]

As an example of an H2TS application, the APEX facility was commissioned by Westinghouse and the DOE in the 1990s to perform design basis accidents for their AP-600 reactor design featuring passive safety systems. In accordance with the H2TS method, the analyzers developed a Phenomena Identification and

Ranking Table (PIRT), and system subdivision [6]. Examples of the APEX system's subdivisions are presented in figures 2.7 and 2.8. Note that in Figure 2.7 RCS stands for Reactor Coolant System, CHF stands for Critical Heat Flux, PZR means Pressurizer, SG stands for Steam Generator, and ϕ stands for phase. In Figure 2.8, ACC means Accumulator, IRWST stands for In-Containment Refueling Water Storage Tank, and PRHR stands for Passive Residual Heat Removal. The system is divided for the purpose of defining specific physical interactions within the systems to be scaled.

The scaling analysis is then performed, first with a top-down approach, and then with a bottom-up approach. The general methods that are observed in the APEX scaling are very similar to those performed in the MASLWR scaling. The process is described in detail in chapter 4, although a bottom-up analysis is not required for this study. The purpose of the top-down analysis is to define characteristic time ratios from the general mass momentum and energy conservation equations for the processes identified in the system subdivision. The time ratios can then be used to rank phenomena for their importance to a given physical process. The bottom-up scaling analysis is intended to provide closure relations for the characteristic time ratios given by the top-down scaling analysis [6].

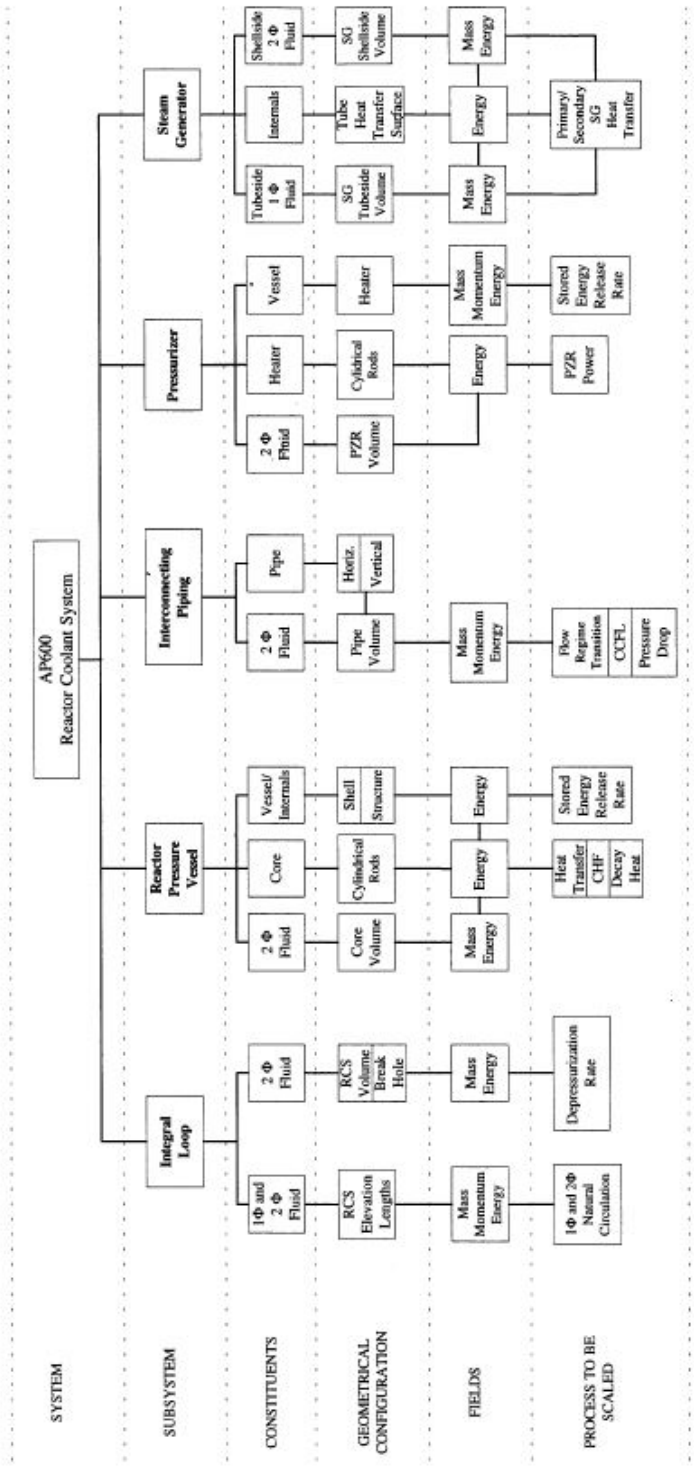

Figure 2.7: APEX subdivision chart for the reactor coolant system [6]

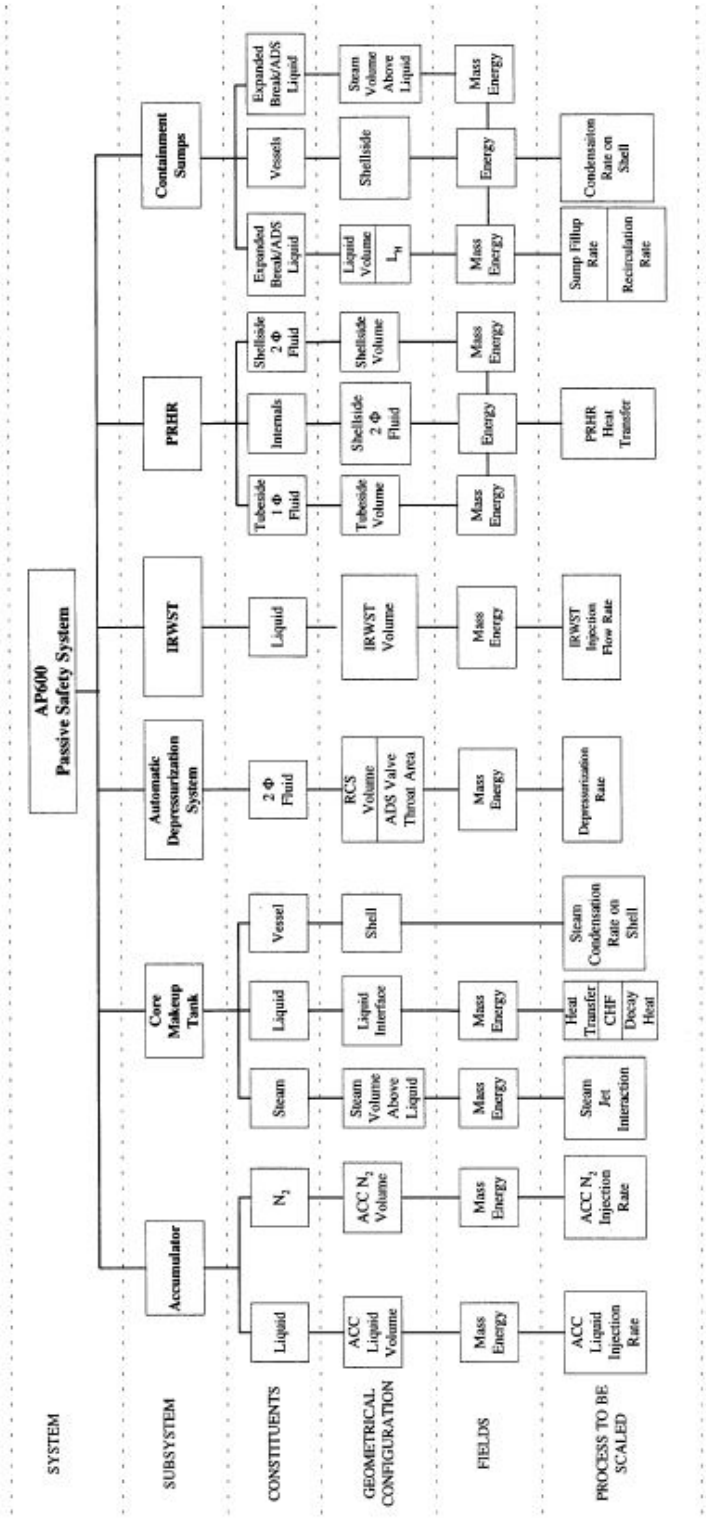

Figure 2.8: APEX subdivision chart for the passive safety system [6]

Chapter 3: MASLWR Facility Description

In order to properly understand the scaling concepts and the RELAP5-3D model, the Oregon State University Multi-Application Small Light Water Reactor (MASLWR) Facility must be well understood. This chapter provides a description of the MASLWR facility and its instrumentation in order to provide sufficient information to understand the nodalization of the RELAP5-3D model created for this study.

3.1 MASLWR Facility

The MASLWR was originally built to run tests to observe natural circulation phenomena in nuclear reactors. The design is that of a natural circulation powered pressurized water reactor. It is an integral system test facility, including a primary system, secondary side, emergency core cooling system, containment vessel, and cooling pool vessel. Each subsystem is instrumented to provide pressure, temperature, flow rate, and power information where appropriate. The specifics of each subsystem are presented in the following subsections.

The naming convention for facility instrumentation is listed here:

- DP - Differential pressure sensor
- LDP - Differential pressure sensor measuring liquid level
- FDP - Differential pressure sensor measuring liquid flow rate
- FCM - Coriolis Flow Meter
- FVM - Vortex Flow Meter

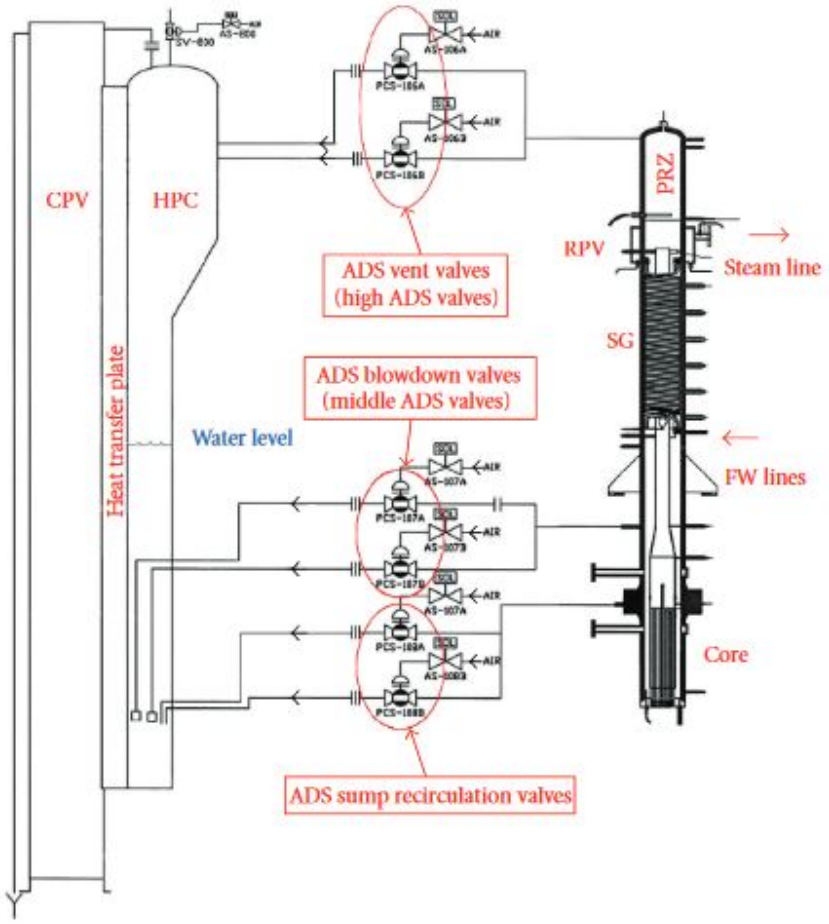

Figure 3.1: MASLWR general layout diagram [7]

- KW - Power transducer
- TF - Thermocouple measuring fluid temperatures
- TW - Thermocouple measuring wall temperatures

3.1.1 Primary System

The primary side of the MASLWR facility consists of the following main components:

- Core Region
- Hot Leg Riser
- Upper Plenum
- Steam Generator Shell
- Downcomer
- Lower Plenum
- Pressurizer

Subcooled liquid is heated in the core region, and rises due to buoyancy forces up through the hot leg riser to the upper plenum. Here, a baffle plate keeps liquid from flowing up into the pressurizer, instead deflecting it down into the steam generator shell where it is cooled by the integral helical coil steam generator. Liquid continues to flow down into the downcomer, and from there into the lower plenum, where it flows back into the core region. The flow is driven entirely by natural circulation with the core as the heat source and the steam generator as the heat sink. The pressurizer operates with a variable heater to maintain system pressure.

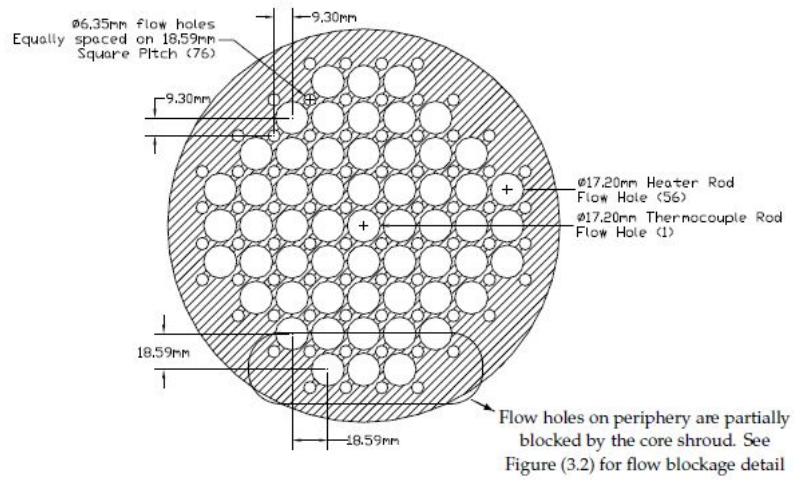

Figure 3.2: MASLWR core arrangement [2]

3.1.1.1 Core Region

The core region is 19.71cm in diameter, and is comprised of fifty-six 73.7cm long, 1.25cm diameter heater rods that supply, at a maximum, 400kW of thermal power to the system; an average value of 7.1kW per rod. The rods are arranged in a 1.86cm pitch square array with 0.635cm diameter auxiliary flow holes around each rod. The arrangement can be seen in Figure 3.2. As is noted in Figure 3.2, the periphery flow holes are partially blocked by the core shroud which blocks up to 3/4 of an auxiliary flow hole, as shown in Figure 3.3. Facility 0 elevation is defined as the top of the core heater rods.

A set of grid wires midway up the core region is employed to keep the rods from deflecting in a way such that the flow characteristics would be distorted. These can be seen in Figure 3.4. A fifty-seventh rod in the center houses 6 thermocouples for measurement of the core temperature gradient. The core instrumentation includes:

- TF-101 (bottom) through TF-106 (top) measure core temperature gradient

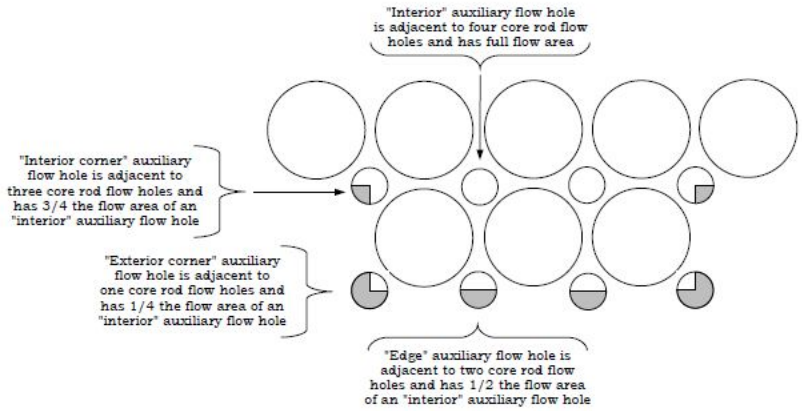

Figure 3.3: Shroud blockages [2]

Figure 3.4: Photograph of MASLWR core region from top [2]

- TF-121 through TF-124 measure core inlet temperature in the lower plenum
- DP-101 measures pressure loss across the core
- LDP-106 measures liquid level in the RPV (not including the pressurizer)
- KW-101 measures half of the power in the core
- KW-102 measures half of the power in the core

3.1.1.2 Hot Leg Riser

The hot leg riser extends above the core section and guides the hot fluid up to the upper plenum. The hot leg riser has few distinguishing characteristics apart from the reducer section, which contracts the diameter from the core region's 19.71cm to 10.23cm over a length of 24.45cm. The hot leg riser also contains a v-cone flow meter for measuring the primary coolant flow rate; FDP-121. The FDP is at an elevation of roughly 60.5cm above facility reference. All instrumentation is listed below:

- TF-132 measures temperature midway up the hot leg riser
- TF-111 measures temperature at the top of the hot leg riser, just before the outlet
- FDP-121 measures primary coolant flow rate
- DP-102 measures pressure loss from core outlet to reducer inlet
- DP-103 measures pressure loss across reducer
- DP-104 measures pressure loss from reducer outlet to upper plenum

3.1.1.3 Upper Plenum

The upper plenum immediately follows the outlet of the hot leg riser section. It is connected to both the pressurizer and the steam generator. Flow is directed into the steam generator shell by the baffle plate that blocks flow from the upper plenum to the pressurizer. Eight 2.54cm holes allow pressure communication with the pressurizer.

3.1.1.4 Steam Generator Shell

The steam generator shell houses the bundle of helical coils that makes up the integral steam generator. Primary coolant flows over the outside of the fourteen 1.59cm diameter tubes that act as the heat sink for the core power. All instrumentation is listed below:

- TF-701 (bottom) through TF-706 (top) measure the primary fluid temperature gradient
- DP-105 measures pressure loss across the upper plenum and the steam generator shell
- DP-107 measures pressure loss across the bottom half of the steam generator shell
- DP-108 measures pressure loss across the upper plenum and top half of the steam generator shell

3.1.1.5 Downcomer

The downcomer carries the fluid from the outlet of the steam generator to the lower plenum. It has few distinguishing features apart from the reducer section that is mirrored from the hot leg riser. It is instrumented as listed below:

- TF-131, 133, and 134 measure temperature azimuthally around the steam generator shell exit
- DP-106 measures pressure loss across the downcomer

3.1.1.6 Lower Plenum

The lower plenum follows the downcomer and completes the primary coolant circuit. Like the upper plenum, the lower plenum deflects flow along the intended path, in this case the core. The unheated portion of the core heater rods comes up through the lower plenum, effectively dividing the lower plenum into the rodded and un-rodded portions. As mentioned previously, TF-121 through TF-124 measure temperature in the lower plenum.

3.1.2 Secondary System

The secondary system of the MASLWR is responsible for acting as the primary heat sink for the primary side. It is composed of the following primary components:

- Feed Water Storage Tank
- Secondary Inlet
- Steam Generator
- Secondary Outlet

Figure 3.5: Photograph of MASLWR steam generator (MASLWR Facility Description report)

3.1.2.1 Feed Water Storage Tank

In order to provide the proper amount of head pressure for the main feed pump, and to ensure a safe margin for facility shutdown in the event that city water pressure is lost, the MASLWR facility is equipped with a feed water storage tank (FWST). Water from the city main supplies the feed water storage tank while the Main Feed Pump (MFP) operates to pump water through the secondary side. The FWST is instrumented with LDP-501 to ensure a safe liquid level is maintained.

3.1.2.2 Steam Generator

The steam generator (SG) is composed of three separate coils of stainless steel tubes. The outer coil and middle coil each have five tubes, while the inner coil has four tubes. It is noteworthy that one of the tubes of the outer coil was accidentally punctured during maintenance of the facility prior to the testing that concerns this study, so the outer coil only has four operational tubes, because the punctured tube was intentionally plugged. The flow direction of the tubes is counter-clockwise for the inner and outer coils, and clockwise for the middle coil. The SG is pictured in figure 3.5.

Feed water from the FWST is forced through the SG via the MFP at roughly atmospheric temperatures and split into the different coils via the inlet header. The inlet header is equipped with variable position needle valves that are kept at five 360° turns open except in specific circumstances. The steam tubes exhaust into a common steam drum where it travels through the main steam line to the "stack", which is a common exhaust line for the entire facility that releases steam to the atmosphere. A variable position regulating valve (MS-504) is installed on the main steam line and allows the operator to set an "auto mode" for the valve to maintain steam line exit pressure. The instrumentation on the secondary side is as follows:

- FMM-501 reads total secondary flow out of the MFP
- FCM-511 through FCM-531 measure flow in each bundle
- FVM-602 measures steam flow rate on the main steam line
- TF-611 through TF-615 measure SG exit temperature in the outer coil
- TF-621 through TF-625 measure SG exit temperature in the middle coil
- TF-631 through TF-635 measure SG exit temperature in the inner coil
- TF-502 measures SG inlet temperature

3.1.3 Automatic Depressurization System

The Automatic Depressurization System (ADS) is used for conduct of testing involving LOCAs. The ADS lines are comprised of a pair of reactor vent lines (upper), a pair of blowdown lines (mid), and a pair of sump return lines (lower). The vent lines penetrate the reactor pressurizer at a height of 374.33 cm above facility reference 0 elevation, the blowdown lines at 66.36 cm, and the sump return lines at 5.40 cm. There is an isolation valve on each line that is pneumatically

actuated from the Data Acquisition and Control System to initialize a steam blow down transient. On either side of each valve is a flow orifice for proper scaling of the flow losses. The lines are formed from a single tee off of the RPV that splits the single RPV penetration into two lines. All lines are horizontally oriented for the entire traverse of the line, and transition from 1.91 cm diameter to 1.27 cm diameter at the tee off of the RPV.

3.1.4 Containment and Cooling Pool Vessels

This section describes the details of the hight pressure containment vessel and cooling pool vessel.

3.1.4.1 High Pressure Containment

The high pressure containment vessel (HPC) is used for containing steam that is released from the RPV through the ADS. All of the lines described in section 3.1.3 connect to this vessel. When steam is injected into the HPC, it heats up and transfers heat through the HTP into the CPV which acts as the ultimate heat sink. The HPC is a vertically oriented vessel that stands at 5.75 m tall and has three sections. The lower section has an outside diameter (OD) of 27.0 cm, with wall thickness 0.318 cm, and height 3.87 cm. The middle section is composed of a cone that expands from 27.0 cm OD to 50.8 cm over a vertical traverse of 20.0 cm. The upper section of the HPC is a 50.8 cm OD cylinder with wall thickness 0.476 cm. The top is capped with a 16.0 cm high, 0.476 cm thick hemispherical head. The vessel is also equipped with four strip heaters attached to the outside of the vessel for maintaining an adiabatic boundary condition It is instrumented in the following way:

- PT-801 measures gauge pressure in the HPC

- LDP-801 measures level in the HPC
- TH-891 through 894 measure temperature of the HPC wall heaters
- TW-891 through 894 measure temperature of the HPC wall near the heaters
- TF-811 through 861 measure fluid temperature up against the heat transfer plate

3.1.4.2 Heat Transfer Plate

The heat transfer plate (HTP) connects the HPC to the cooling pool vessel (CPV), representing the heat transfer area between the containment and the cooling pool of the conceptual design. The HTP is welded to both the HPC and the CPV, and traverses the entire vertical height of the HPC less the hemispherical cap (5.59 m). It is 16.8 cm wide, 3.81 cm thick, and is made of SS304 grade steel. The instrumentation is as follows:

- TW-812 through TW-862 measure HTP temperature on the HPC side
- TW-813 through TW-863 measure midline HTP temperature
- TW-814 through TW-864 measure HTP temperature on the CPV side

3.1.4.3 Cooling Pool Vessel

The CPV is a simple open tank composed of SS304 grade steel, and is covered in 5.08 cm of Thermo-12 hydrous calcium silicate insulation. The tank measures 7.37 m tall, 76.2 cm OD, and 0.635 cm wall thickness. The CPV is instrumented as follows:

- LDP-901 measures level in the CPV

- TF-815 through 865 measure fluid temperature up against the heat transfer plate
- TF-892 measures temperature at the top of the CPV

3.2 Data Collection and System Control

Data is collected and stored on the OSU MASLWR Data Acquisition and Control System (DACS). The system processes input signals from instrumentation, and logs their readings in a text file for later analysis. The system utilizes various field (I/O) modules, along with a programmable logic controller (PLC), a desktop computer, an Analog to Digital Converter (ADC), and the Entivity Studio 7.0 software. The software on the computer acts as the graphical user interface for operating the facility. Various safety trips are programmed into the code to prevent over-pressurization and/or overheating of various components, and other unsafe conditions. These safety trips are designed to prevent damage to the facility, and harm to facility personnel. Instrument measurement uncertainties for the MASLWR facility are presented in figure 3.6 [2].

Instrument Type	Tag Number	Uncertainty
Vortex flow meter	FVM-602	1.5% of indicated value
Coriolis flow meter	FCM-511, -521, -531	0.5% of indicated value
Magnetic flow meter	FMM-501	0.5% of indicated value
Thermocouple	Various; TW-xxx, TF-xxx, TH-xxx	±3.2°C
Pressure meter	PT-511, -521, -531	2.1 psi[a]
Pressure meter	PT-301	7.0 psi[a]
Pressure meter	PT-602	1.75 psi[a]
Pressure meter	PT-801	1.4 psi[a]
Differential pressure meter	DP-101, -104, -106	0.0875 inches H_2O[a]
Differential pressure meter	DP-102	0.007 inches H_2O[a]
Differential pressure meter	DP-103, -105	0.035 inches H_2O[a]
Flow differential pressure meter	FDP-131	0.0875 inches H_2O[a]
Level differential pressure meter	LDP-106	0.517 inches H_2O[a]
Level differential pressure meter	LDP-301	0.086 inches H_2O[a]
Level differential pressure meter	LDP-501, -901	0.875 inches H_2O[a]
Level differential pressure meter	LDP-801	0.772 inches H_2O[a]
Level differential pressure meter	LDP-601	0.0525 inches H_2O[a]
Power meter	KW-101, -102,	0.6% of indicated value

[a]Uncertainty is 0.35% of instrument upper range value.

Figure 3.6: MASLWR instrument uncertainties [2]

Chapter 4: Scaling Methodology

As previously stated, one of the main goals of this research is to establish a revised set of scaling parameters for the OSU-MASLWR facility. This is necessary for one primary reason: the core heater assembly installed in the MASLWR facility was not capable of reaching the appropriate level of heat to apply the existing MASLWR scaling parameters in full power testing. This was deemed acceptable in the past due to the fact that decay power levels could still be adequately simulated, since the primary objective of the facility was accident testing (i.e. scram conditions). Since the current research addresses steady state, full power, and load following operations, however, the existing MASLWR scaling report, reference [8], cannot be applied. What remains then is to create a new set of scaling parameters which relate the actual full power to the already established relations of the existing MASLWR scaling report.

Bearing this in mind, we must first consider the state of the MASWLR facility. As mentioned in chapter 3, the MASLWR facility was decommissioned in late July of 2014, at which point the facility was almost entirely dismantled. This provides its own set of challenges in regard to how the previous data, and any new adjustments to the scaling, must be handled. The most notable challenges include:

- All geometric scaling factors are fixed.
- Maximum core power is fixed.
- The facility is not available for examination.
- Realistically limited to Hierarchical Two-Tiered Scaling methodology (same as MASLWR).

- Required to make at least the same assumptions as original MASLWR scaling report, and possibly additional assumptions.

With these limitations known, we move forward with the analysis. In the original MASLWR scaling, the approach was Hierarchical Two-Tiered Scaling (H2TS). The H2TS method typically involves the steps presented in Figure 4.1:

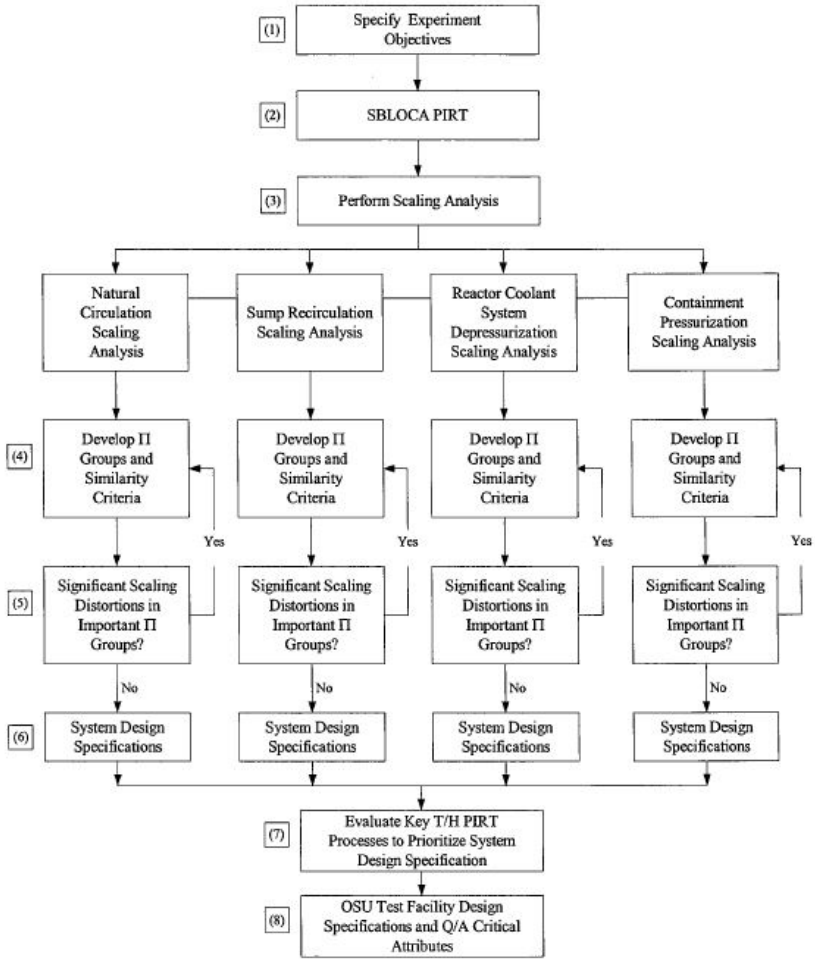

Figure 4.1: MASLWR general scaling method for Small Break Loss of Coolant Accidents (SBLOCA) [8]

Due to the limitations listed above, very few of these steps actually hold up in this situation. Most notably, steps 2, 6, 7, and 8 from Figure 4.1 cannot be performed because we have no ability to make design adjustments to the facility. Given the fixed parameters, there is no function of a PIRT for this analysis because the design cannot be tailored to fit it. This also forces certain assumptions on the analysis that were present with the MASLWR facility's original scaling analysis that must be carried through for the new set of scaling parameters to be realistic. The MASLWR scaling analysis can be viewed in detail in reference [8].

4.1 Single-Phase Natural Circulation Scaling

The single phase natural circulation scaling is performed in accordance with the H2TS scaling: top-down analysis followed by bottom-up analysis. The top-down portion seeks to identify important processes by way of non-dimensionalizing the conservation equations. Each non-dimensional group, or Π group, represents the relative magnitude of each term. If facility design parameters were being adjusted based on scaling distortions, this is one of the primary ways that phenomena are ranked.

We begin with a general conservation equation for mass, one for momentum, and one for energy. All of these can take the following form, taken from reference [8]:

$$\frac{dV_k\psi_k}{dt} = [Q_k\psi_k]_{in} - [Q_k\psi_k]_{out} + \sum (j_{kn}A_{kn}) + S_k \tag{4.1}$$

Where ψ_k represents any of the following:

- ρ (mass)
- ρu (momentum)
- ρe (energy)

and other variables are itemized below:

- k = constituent
- V_k = volume of constituent
- Q_k = volume flow rate through constituent
- j_{kn} = flux of ψ_k transferred from k to n
- A_{kn} = area over which j_{kn} is transferred
- S_k = source term for constituent

In this case, a "constituent" refers to a portion of the loop of interest (e.g. core region of primary loop). Equation (4.1) is non-dimensionalized to identify the significant processes through what are called Pi groups. The non-dimensionalization is carried out by first defining non-dimensional variables:

$$V_k = V_k^+ V_{k,0} \tag{4.2}$$
$$\psi_k = \psi_k^+ \psi_{k,0} \tag{4.3}$$
$$Q_k = Q_k^+ Q_{k,0} \tag{4.4}$$
$$j_{kn} = j_{kn}^+ j_{kn,0} \tag{4.5}$$
$$A_{kn} = A_{kn}^+ A_{kn,0} \tag{4.6}$$
$$S_k = S_k^+ S_{k,0} \tag{4.7}$$

A "+" in equations (4.2) through (4.7) denotes a non-dimensional parameter. These relations are substituted into equation (4.1) to put it in terms of the non-dimensional parameters. Note that going forward, the following simplification is made: $[Q_k\psi_k]_{in} - [Q_k\psi_k]_{out} = \Delta Q_k \psi_k$. This expression is much more useful for the non-dimensional form of equation (4.1).

$$V_{k,0}\psi_{k,0}\frac{dV_k^+\psi_k^+}{dt} = Q_{k,0}\psi_{k,0}\Delta Q_k^+\psi_k^+ \ + \sum j_{kn,0}A_{kn,0}\left(j_{kn}^+A_{kn}^+\right) + S_{k,0}S_k^+ \tag{4.8}$$

Equation (4.8) simplifies to the following when dividing by $Q_{k,0}\psi_{k,0}$:

$$\tau_k\frac{dV_k^+\psi_k^+}{dt} = \Delta Q_k^+\psi_k^+ \ + \sum \Pi_{kn}\left(j_{kn}^+A_{kn}^+\right) + \Pi_{sk}S_k^+ \tag{4.9}$$

where

$$\tau_k = \frac{V_{k,0}}{Q_{k,0}} \tag{4.10}$$

$$\Pi_{kn} = \frac{j_{kn,0}A_{kn,0}}{Q_{k,0}\psi_{k,0}} \tag{4.11}$$

$$\Pi_{ks} = \frac{S_{k,0}}{Q_{k,0}\psi_{k,0}} \tag{4.12}$$

τ_k (equation (4.10)) is known as the *mean residence time*. It represents the mean time that a process has to occur in the constituent k. Π_{kn} (equation (4.11)) is the characteristic time ratio for transfer processes occurring between constituents k and n. Finally, the characteristic time ratio for the source term (equation (4.12)) is represented by Π_{ks}. Using these Pi groups, the different processes can be ranked by importance. If the value of a Pi group is shown to be much less than 1, this implies very little importance to the overall process of the control volume. Predictably, the opposite is true of a Pi value that is much greater than 1. It is also useful to define the Pi group ratio, equation (4.13), as this is the primary way in which the scaling factors are presented for this study.

$$\Pi_R = \frac{\Pi_m}{\Pi_p} \tag{4.13}$$

4.1.1 Definition of Scaling Pi Groups

In order to define the specific Pi groups for the single phase natural circulation, we must first define the conditions to which the processes will be scaled. Since the adjusted scaling parameters are necessary only for full power testing that will likely not vary far from steady state, it makes sense to scale to steady state conditions like the original MASLWR scaling. With this decided, governing equations are developed for steady state:

- Conservation of mass
- Conservation of momentum
- Conservation of energy

Starting with equation (4.1), we first construct the conservation of mass equation. This is constructed assuming the following:

- Steady state
- Incompressible
- No mass leaves or enters loop
- Boussinesq approximation [8]

Note assuming steady state allows for the scaling ratios of the loop flow losses and buoyancy terms to be scaled to values other than 1:1, allowing reduced power scaling. With these assumptions, we are only left with the convective terms of the mass conservation equation. Using the core as a reference point, we define the mass flow rates for each section of the flow loop:

$$\frac{d\rho_l V}{dt}_i = \rho_l (Q_{in} - Q_{out})_i \tag{4.14}$$

Applying this equation to a given cross section in the loop:

$$\rho_l u_c A_c = \rho_l u_i A_i \tag{4.15}$$

where the subscript "c" refers to the core, and the subscript "i" refers to any given portion of the primary circuit. This equation doesn't define any Pi groups for the purpose of scaling, but it does help define a useful relation for fluid velocities over the entire loop:

$$u_i = u_c \frac{A_c}{A_i} \tag{4.16}$$

The next equation to be defined is the momentum conservation equation for a single component:

$$\frac{d\rho_l u_i l_i}{dt} = \rho_l (u_{in}^2 - u_{out}^2)_i + g L_{th} (\rho_l - \rho_h)_i - \frac{\rho_l u_i^2}{2} \left(\frac{fl}{d_H} + K \right)_i \tag{4.17}$$

The density term can be simplified to the more well-known representation presented in equation (4.18)

$$\frac{d\rho_l u_i l_i}{dt} = \rho_l (u_{in}^2 - u_{out}^2)_i + \beta g \rho_l \Delta T L_{th} - \frac{\rho_l u_i^2}{2} \left(\frac{fl}{d_H} + K \right)_i \tag{4.18}$$

where the variables are defined as the following:

- ρ_l = average fluid density
- u_i = area averaged fluid velocity of component "i"
- l_i = length of component "i"
- t = time
- g = gravity constant

- β = thermal expansion coefficient
- L_{th} = characteristic thermal length of loop
- ΔT = change in temperature over entire loop
- f = Darcy friction factor
- d_H = hydraulic diameter
- K = dimensionless form loss factor

Since the goal is to scale the entire loop, equation (4.18) must be integrated over the entire loop. This essentially becomes a summation of all of the terms in the equation for each component in the loop. For the purpose of simplifying the equation, all fluid velocities are written in terms of the core velocity by substituting equation (4.16) into equation (4.18). The result is presented in equation (4.19):

$$\sum_{i=1}^{N} l_i \frac{A_c}{A_i} \frac{d\rho_l u_c}{dt} = \beta g \rho_l \Delta T L_{th} - \frac{\rho_l u_c^2}{2} \sum_{i=1}^{N} \left(\frac{fl}{d_H} + K \right)_i \left(\frac{A_c}{A_i} \right)^2 \tag{4.19}$$

Equation (4.19) represents the momentum equation to be scaled. This requires that the equation be non-dimensionalized to construct a portion the Pi groups that govern the overall process. Note that $\rho_l u_{c0}^2$ is the term that we divide through by. This is classically done to derive the proper Pi groups.

$$\frac{\sum_{i=1}^{N} l_i \frac{A_c}{A_i}}{u_{c,0}} \frac{du_c^+}{dt} = \frac{\beta g \Delta T_0 L_{th}}{u_{c,0}^2} \Delta T^+ - \frac{1}{2} \sum_{i=1}^{N} \left(\frac{fl}{d_H} + K \right)_i \left(\frac{A_c}{A_i} \right)^2 u_c^{2^+} \tag{4.20}$$

The momentum equation Pi groups are listed below:

$$\tau = \frac{\sum_{i=1}^{N} l_i \frac{A_c}{A_i}}{u_{c,0}} \tag{4.21}$$

$$\Pi_F = \sum_{i=1}^{N} \left(\frac{fl}{d_H} + K \right) \left(\frac{A_c}{A_i} \right)^2 \tag{4.22}$$

$$\Pi_{Ri} = \frac{\beta g \rho_l \Delta T_0 L_{th}}{u_{c,0}^2} \tag{4.23}$$

Next, we move to the energy equation in order to complete the collection of single phase natural circulation scaling parameters. The same general process will apply, where we begin with the energy equation for a single loop component:

$$\frac{d(\rho_l c_{v,l} T_l V_l)_i}{dt} = (\rho_l c_{p,l} \Delta T_l Q_l)_i + q_i \tag{4.24}$$

Where the variables are defined as the following:

- ρ_l = average fluid density
- $c_{v,l}$ = constant volume specific heat
- $c_{p,l}$ = constant pressure specific heat
- $T_{l,i}$ = bulk fluid temperature of component
- $V_{l,i}$ = component volume
- t = time
- $Q_{l,i}$ = volumetric flow rate in component
- q_i = given heat transfer process into or out of component

As with the momentum equation, we wish to scale the energy equation to the entire loop, not on a per component basis. To this end, we integrate equation (4.24) to obtain the appropriate energy balance for the entire loop.

$$\frac{d\rho_l c_{v,l} T_l V_l}{dt} = q_{core} - q_{SG} - q_{loss} \tag{4.25}$$

This equation is expanded to equation (4.26) using the relations for q_{core} and q_{SG}:

$$\frac{d\rho_l c_{v,l} T_l V_l}{dt} = \dot{m}_{pri} c_{p,l} \Delta T_{core} - U_{SG} A_{SG} \Delta T_{SG} - q_{loss} \tag{4.26}$$

Next, the equation is non-dimensionalized by dividing out by the quantity $q_{core,0}$:

$$\frac{c_{v,l} M_l}{c_{p,l} \dot{m}_{pri}} \frac{dT_l^+}{dt} = \dot{m}_{pri}^+ \Delta T_{core}^+ - \frac{U_{SG,0} A_{SG} \Delta T_{SG,0}}{q_{core,0}} U_{SG}^+ \Delta T_{SG}^+ - \frac{q_{loss,0}}{q_{core,0}} q_{loss}^+ \tag{4.27}$$

It will be shown later that the steam generator heat transfer coefficient U_{SG}, and the steam generator temperature change, ΔT_{SG}, are not individually scaled. The primary reason for this is that the exact heat transfer characteristics of the helical coil steam generator are unknown. Limited correlations exist to characterize heat transfer coefficients of helical coil heat exchangers, which necessitates a more creative solution to the notion of scaling this process. This was achieved in the original MASLWR scaling by assuming that the secondary side mass flow rate would be varied as needed to maintain steady state. That is to say, the total heat flux is scaled, as opposed to the individual variables that make up the heat flux. The same technique will be applied here, as there is no realistic way to obtain specific data on the heat transfer characteristics of the MASLWR steam generator. Note also that the $\frac{q_{loss,0}}{q_{core,0}}$ term is assumed to be insignificant due to insulation on the facility, but its Pi group is included for completeness. Presented below is a

list of the Pi groups derived from the energy equation for the loop. Table 4.1 summarizes all of the relevant Pi groups.

$$\tau = \frac{M_{loop,0}}{\dot{m}_{loop,0}} \tag{4.28}$$

$$\Pi_{SG} = \frac{U_{SG,0} A_{SG} \Delta T_{SG,0}}{q_{core,0}} \tag{4.29}$$

$$\Pi_{loss} = \frac{q_{loss,0}}{q_{core,0}} \tag{4.30}$$

Π Group	Equation	Physical Meaning
τ	$\frac{M_{loop,0}}{\dot{m}_{loop,0}}$	Mean residence time
Π_F	$\sum_{i=1}^{N} \left(\frac{fl}{d_H} + K \right) \left(\frac{A_c}{A_i} \right)^2$	Overall flow losses
Π_{Ri}	$\frac{\beta_0 g \rho_{l,0} \Delta T_0 L_{th}}{u_{c,0}^2}$	Richardson number: ratio of buoyancy to flow gradient
Π_{SG}	$\frac{U_{SG,0} A_{SG} \Delta T_{SG,0}}{q_{core,0}}$	Steam generator heat sink to core power ratio
Π_{loss}	$\frac{q_{loss,0}}{q_{core,0}}$	Ambient heat losses to core power ratio

Table 4.1: Π group accounting

4.1.2 Derivation of Single-Phase Scaling Factors

In order to understand the definitions of the scaling factors, we must first recall equation (4.13). The scaling factors are determined by these ratios. It is also important to recall from the beginning of this chapter that many of these distortions are already fixed, such as the geometric and flow loss scaling factors, and from this information, determine what we have left to define with the modified core power scaling factor. For the convenience of the reader, accountings of the original scaling

ratios, the fixed scaling ratios, and those left to be defined are presented in tables 4.2, 4.3, and 4.4, respectively.

Scaling Ratio	Scaling Factor	Physical Meaning
L_R	$\frac{1}{3.1}$	Length scaling factor
$L_{SG,R}$	$\frac{1}{3.1}$	Steam generator length scaling factor
A_R	$\frac{1}{82.2}$	Cross-sectional area scaling factor
$A_{SG,R}$	$\frac{1}{254.7}$	Steam generator heat transfer area scaling factor
V_R	$\frac{1}{254.7}$	Volume scaling factor
$\left(\frac{A_c}{A_i}\right)_R$	1	Flow area change ratio
$\Pi_{F,R}$	3.1	Flow loss scaling factor
$Prop_R$	1	Scaling ratio of *all* fluid properties
$\Pi_{SG,R}$	1	Steam generator heat transfer scaling factor
τ_R	1	Time scaling factor
$q_{core,R}$	$\frac{1}{254.7}$	Core power scaling factor
u_R	$\frac{1}{3.1}$	Velocity scaling factor
$\Delta T_{core,R}$	1	Core temperature change scaling factor
$(U_{SG}\Delta T_{SG})_R$	1	Heat transfer coefficient scaling ratio

Table 4.2: Original MASLWR scaling ratios

Scaling Ratio	Scaling Factor	Physical Meaning
L_R	$\frac{1}{3.1}$	Length scaling factor
$L_{SG,R}$	$\frac{1}{3.1}$	Steam generator length scaling factor
A_R	$\frac{1}{82.2}$	Cross-sectional area scaling factor
$A_{SG,R}$	$\frac{1}{254.7}$	Steam generator heat transfer area scaling factor
V_R	$\frac{1}{254.7}$	Volume scaling factor
$\left(\frac{A_c}{A_i}\right)_R$	1	Flow area change ratio
$\Pi_{F,R}$	3.1	Flow loss scaling factor
$Prop_R$	1	Scaling ratio of *all* fluid properties
$\Pi_{SG,R}$	1	Steam generator heat transfer scaling factor

Table 4.3: Fixed scaling ratios

Scaling Ratio	Physical Meaning
τ_R	Time scaling factor
$q_{core,R}$	Core power scaling factor
u_R	Velocity scaling factor
$\Delta T_{core,R}$	Core temperature change scaling factor
$(U_{SG}\Delta T_{SG})_R$	SG heat flux scaling factor

Table 4.4: Scaling ratios to be defined

A careful review of the MASLWR scaling report will reveal that for the previous set of scaling parameters, $\Pi_{F,R}$ was also equal to 3.1. In theory, as the fluid velocity scaling factor changes (as it will in this new set of scaling parameters), so too would the Darcy friction factor. This would mean that for the new set of scaling parameters, $\Pi_{F,R}$ would not be equal to 3.1. While this is strictly true, the general practices of scale models cause the form loss factor K to dominate the magnitude of Π_F. Since with shorter pipes the friction loss is less than that of the prototype, orifices and other obstructions are added to the flow path to create the proper total pressure loss. Combining this practice with the large form loss factors from the

core region, v-cone flow meter section, upper and lower plenums, and the steam generator region, the form factor loss coefficients clearly dominate Π_F. Based on this reasoning, the previous scaling factor for $\Pi_{F,R}$ shall be kept as a constraint to solve for the new set of scaling parameters.

The first scaling ratio that must be defined for the analysis is the core power scaling factor $q_{core,R}$. This too is derived using information from the MASLWR scaling report. It is stated that the core full power for the MASLWR would need to be 591 kW in order to be properly scaled [8]. However, the provided full power is only 400 kW. Thus the new core power scaling ratio can be determined by applying this ratio to the existing core power ratio of $q_{core,R} = \frac{1}{254.7}$.

$$q_{core,R} = \frac{1}{254.7}\frac{400kW}{591kW} = \frac{1}{376.39} \tag{4.31}$$

The next scaling ratio we wish to define is u_R. From the steady state version of equation (4.20), we can see that if we take the model to prototype ratio of the equations, that we get the following relation:

$$\left(\frac{\beta g \Delta T_{core} L_{th}}{u_c^2}\right)_R = \left(\sum_{i=1}^{N}\left(\frac{fl}{d_H} + K\right)_i \left(\frac{A_c}{A_i}\right)^2\right)_R \tag{4.32}$$

Making the following substitution for ΔT_0:

$$\Delta T_{core,R} = \left(\frac{q_{core}}{\rho_l u_c A c_p}\right)_R \tag{4.33}$$

and solving for u_R, equation (4.32) becomes:

$$u_R = \left(\frac{\beta q_{core} L}{\rho_l c_p A \Pi_F}\right)_R^{1/3} \tag{4.34}$$

$$u_R = \frac{1}{3.53} \tag{4.35}$$

Now that the velocity ratio is known, we can also define the new time scaling ratio, τ_R:

$$t_R = \frac{L_R}{u_R} \tag{4.36}$$

$$t_R = 1.14 \tag{4.37}$$

Another scaling ratio to be defined is the core temperature change $\Delta T_{core,R}$. From equation (4.33) we calculate the following:

$$\Delta T_{core,R} = \frac{1}{1.30} \tag{4.38}$$

It is worthy to note here that the change in $\Delta T_{core,R}$ does not adhere to the assumption of identical fluid properties because it results in different temperatures than that of the prototype. For subcooled liquid water, a small sensitivity study was performed at normal MASLWR operating conditions to observe the potential effects. For the worst case scenario of the entire difference in temperature contributing to a higher T_H or lower T_C (rather than both the high and low temperatures equally changing) the difference in fluid density was roughly 2%. This is considered insignificant; hence, the fluid property ratios are considered to still be unity.

Finally, the steam generator heat transfer Pi group must be investigated. It can be seen that for steady state conditions for equation (4.26), $\Pi_{SG,R} = 1$. Under the previous scaling analysis, it was asserted that the scaling ratio of the product of the convective heat transfer coefficient and the temperature change across the

steam generator would be equal to 1: $(U_{SG}\Delta T_{SG})_R = 1$. This argument was made on the basis that the secondary side flow rate would be adjusted to meet these conditions. This forced $A_{SG,R} = \frac{1}{254.7}$ due to the core power scaling ratio. For the current set of scaling parameters, however, $(U_{SG}\Delta T_{SG})_R$ is solved for below:

$$(U_{SG}\Delta T_{SG})_R = \frac{q_{core,R}}{A_{SG,R}} \tag{4.39}$$

so that

$$(U_{SG}\Delta T_{SG})_R = \frac{1}{1.48} \tag{4.40}$$

Thus all of the variable scaling factors for single phase flow have been defined. A final tabulation of all of the relevant scaling factors is presented in table 4.4:

Scaling Ratio	Scaling Factor	Physical Meaning
L_R	$\frac{1}{3.1}$	Length scaling factor
$L_{SG,R}$	$\frac{1}{3.1}$	Steam generator length scaling factor
A_R	$\frac{1}{82.2}$	Cross-sectional area scaling factor
$A_{SG,R}$	$\frac{1}{254.7}$	Steam generator heat transfer area scaling factor
V_R	$\frac{1}{254.7}$	Volume scaling factor
$\left(\frac{A_c}{A_i}\right)_R$	1	Flow area change ratio
$\Pi_{F,R}$	3.1	Flow loss scaling factor
$Prop_R$	1	Scaling ratio of *all* fluid properties
$\Pi_{SG,R}$	1	Steam generator heat transfer scaling factor
τ_R	1.14	Time scaling factor
$q_{core,R}$	$\frac{1}{376.39}$	Core power scaling factor
u_R	$\frac{1}{3.53}$	Velocity scaling factor
$\Delta T_{core,R}$	$\frac{1}{1.30}$	Core temperature change scaling factor
$(U_{SG}\Delta T_{SG})_R$	$\frac{1}{1.48}$	Heat transfer coefficient scaling ratio

Table 4.5: Newly defined scaling ratios

4.2 Applicability and Two-Phase Flow

It is noteworthy that it is well within the realm of possibility to experience subcooled boiling in the MASLWR facility core, especially at the elevated power level for this scaling analysis. Unfortunately, due to the proprietary nature of the NuScale prototype core design, the necessary information could not be acquired to ensure proper scaling of two-phase flow phenomena. As a result, the new scaling analysis is only applicable to single phase flow conditions. To ensure single phase flow in analyses that would apply this scaling analysis, we will determine a criteria for the subcooled margin, as this most directly applies to whether or not two-phase flow will be observed. This will be a best estimate study due to a lack of proper

information on the core, so standard industry practice and conservative estimates will be used.

To begin, we need to establish a basic method: find a way to ultimately relate wall temperature to saturation temperature, and then saturation temperature to core outlet temperature. This will allow us to establish an estimate for the subcooled margin, where the subcooled margin is defined in equation (4.41). To begin, we need to perform a hot channel analysis to establish a relation to calculate wall temperature, which in turn involves calculating the heat transfer coefficient. To calculate the heat transfer coefficient, the Dittus-Boelter equation will be employed:

$$T_{sub} = T_{sat} - T_{out} \tag{4.41}$$

$$Nu = 0.023 Re_{subchannel}^{0.8} Pr^{0.4} \tag{4.42}$$

where

$$Nu = \frac{hD_h}{k_l} \tag{4.43}$$

$$Re_{subchannel} = \frac{\rho_l u_{subchannel} D_h}{\mu_l} \tag{4.44}$$

$$Pr = \frac{\mu_l c_p}{k_l} \tag{4.45}$$

It is most useful to evaluate at the MASLWR's full power of 400kW, a typical operating pressure and T_{out} of 8.62 $[MPa]$ and 522.0 $[K]$, respectively, and a reasonable flow rate at such a power. Unfortunately, there is no usable flow rate data at this power level, so SP-3 data will be used to calculate, using a best fit line, what the mass flow rate might be at 400kW. Moving forward with the analysis, we calculate the following:

$$\begin{aligned}
\dot{m}_{core} =& 2.484 \left[\frac{kg}{s}\right] \\
Re_{subchannel} =& 26553.9 \\
Pr =& 0.8377 \\
D_h =& 9.74E-03 \ [m] \\
k_l =& 0.6169 \left[\frac{W}{m-k}\right] \\
h =& 4699.7 \left[\frac{W}{m^2-k}\right]
\end{aligned}$$

Using the newly calculated heat transfer coefficient, we use the standard convective heat flux equation at the core outlet temperature of $T_{out} = 522.0 \ [K]$ to calculate wall temperature:

$$q" = h(T_{wall} - T_{out}) \tag{4.46}$$

Now that we can relate the wall temperature to the outlet temperature at these conditions, so we only require a relationship between wall temperature and saturation temperature at the onset of subcooled boiling. For a typical cylindrical geometry, Todreas and Kazimi present an equation in Nuclear Systems, Vol. 1, Thermal Hydraulic Fundamentals [23]. For the limit of the onset of nucleate boiling, equation (4.47) is used. In order to use this equation, we must assume that the MASLWR core heater rods have large enough microcavities to induce subcooled boiling.

$$(T_{wall} - T_{sat}) = \left(\frac{8\sigma T_{sat} v_g q"}{k_l h_{fg}}\right)^{1/2} \tag{4.47}$$

Combining the result of (4.47) with a rearranged version of equation (4.46), we set up the following equations to calculate the appropriate subcooled margin to maintain single phase flow:

$$\begin{aligned} T_{wall} - T_{sat} =& 17.91\ [K] \\ T_{wall} =& T_{out} + 53.0\ [K] \\ T_{out} - T_{sat} + 53.0\ [K] =& 17.91\ [K] \end{aligned}$$

Given equation (4.41), the subcooled margin is

$$T_{sub} = 35.1\ [K]$$

So this best estimate method reveals that the proper subcooling margin is $T_{sub} = 35.1\ [K]$, or 63.2 $[F]$. At conditions seen in SP-3, all flow should be single phase. Again, this criteria was calculated using correlations that are not specific to the MASLWR core, but are used in standard industry practice. It is intended to give a conservative estimate of the subcooled margin required for single phase flow. Values utilized here also include the estimated core flow rate of 2.48 $\left[\frac{kg}{s}\right]$ and typical operating pressures and temperatures stated above.

Chapter 5: RELAP5-3D Methods and Results

One of the primary objectives of this thesis is to model the MASLWR system as best as possible in RELAP5-3D. This MASLWR model was adapted from an existing MASLWR model that was developed in the early stages of facility testing. The original model was not strictly validated against test data, so many changes had to be made to make it functional. The testing used to develop the model for this study was the International Atomic Energy Agency's (IAEA's) set of testing for the International Collaborative Standard Problem (ICSP). Specifically, the test in question is SP-3. Given that the primary application of this model is to perform studies with load following applications, SP-3 was the most fitting test to attempt to model. Both the test and the model are described in this chapter, along with the RELAP model results.

5.1 SP-3 Test

According to the official IAEA report of the ICSP testing, reference [22], SP-3 was developed to observe and characterize primary circuit natural circulation flow for different core powers. In the original procedure, the system was brought to steady state natural circulation conditions at varying core powers. The power was first set to 10% and ramps up in increments of 10% up to a maximum power of 80%. Steady state was determined by the following parameters:

- Constant hot leg temperature measured by TF-106 ($\pm 2.8 \deg C$)
- Constant cold leg temperature measured by TF-131 ($\pm 2.8 \deg C$)
- Constant primary flow rate measured by FDP-131 ($\pm 5\%$)

IAEA-TECDOC-1733 reports on a few issues experienced during SP-3. One of the most notable issues was the fact that after the test, during the evaluation of the data, it was determined that while the above conditions were met at each power level, other conditions weren't necessarily being held at steady state, thus the test was strictly a failure. Additionally, there was a lack of adherence to the procedure involving the secondary side outlet conditions. In the procedure, the operators are instructed to adjust secondary flow controls to maintain saturated conditions at the outlet of the steam generator. This was not performed by the test operators during SP-3. The last procedural deviation was the utilization of the coolant charging pump during the test. The coolant charging pump injects coolant from the FWST directly into the lower plenum of the reactor pressure vessel, and can have significant effects on the thermodynamics of the system if utilized during a test. Likely due to minor facility leaks that dropped pressurizer operating level below acceptable limits, the coolant charging pump was activated at short intervals throughout the middle of the test. The effects are minor, but this is included in the RELAP5-3D model. Figures 5.1 through 5.4 show some of the main thermodynamic quantities that define the behavior and objective of the test.

Figure 5.1 shows the power stepping throughout the test. Again, power maneuvering was the focus of SP-3, and the power and flow rate behaved as expected. Figure 5.2 displays the core inlet and outlet temperatures throughout SP-3. These, coupled with figure 5.3, are a good representation of the thermodynamic state throughout the power maneuvering. It can be seen that a large disturbance to the system occurred at roughly 3000 seconds, which lines up well with deliberate operator action to lower the secondary side temperature to be closer to saturated conditions, as noted in the test log [24]. This transient behavior led to the elongated attempt at steady state at the 200 kW level. Overall, SP-3 was not run according to procedure due to a failure to achieve steady state with some system parameters throughout the test.

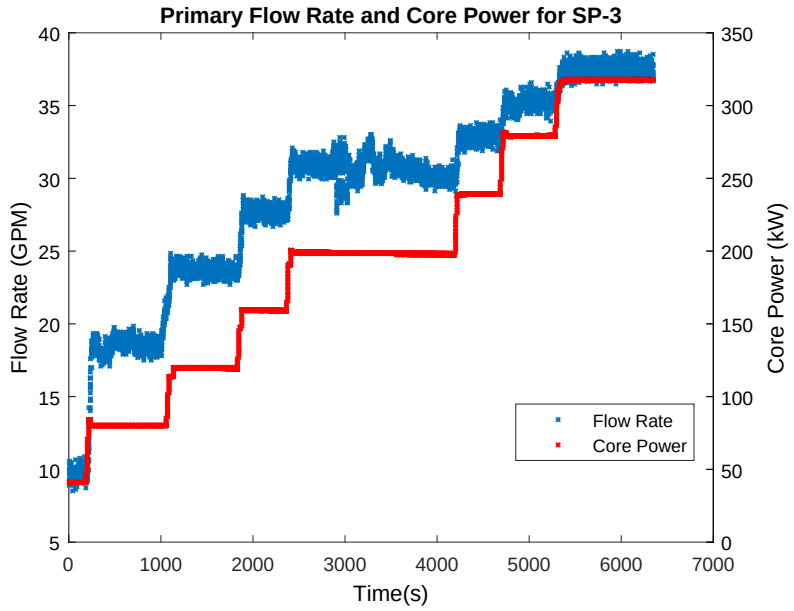

Figure 5.1: Core power and primary volume flow rate during SP-3

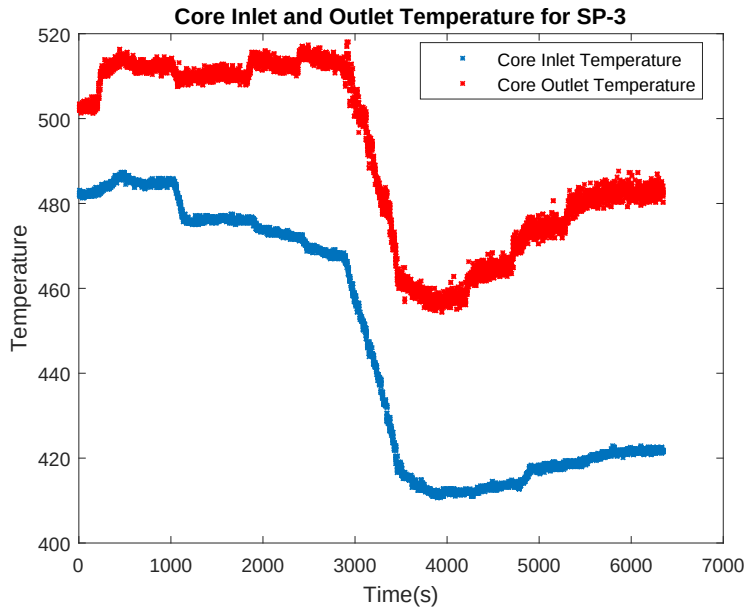

Figure 5.2: Core inlet and outlet temperature during SP-3

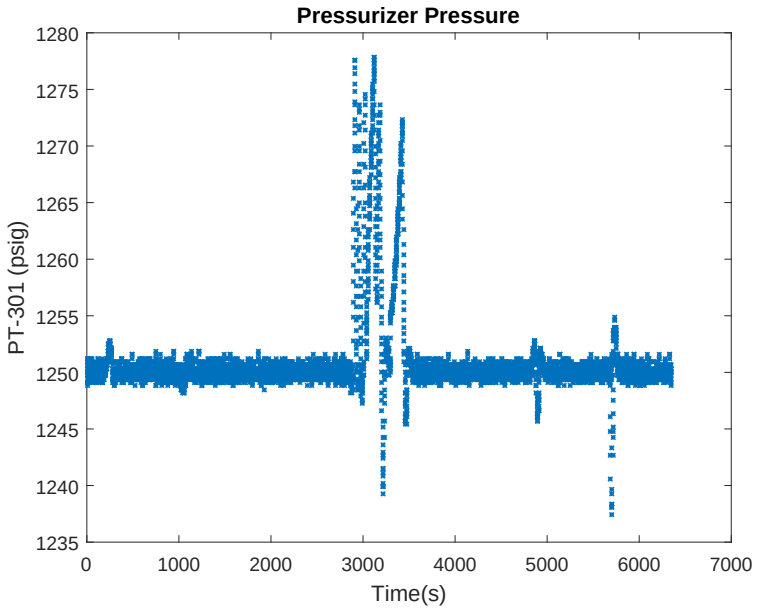

Figure 5.3: System pressure during SP-3

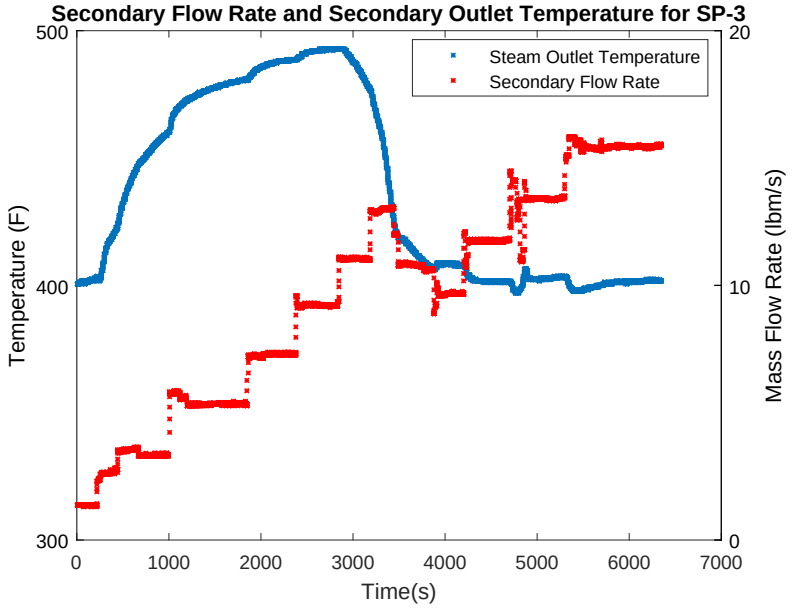

Figure 5.4: Secondary side conditions during SP-3

5.2 RELAP5-3D Model

Since the MASLWR has been decommissioned, dimensions had to be taken from the OSU-MASLWR Facility Description Report and the OSU-MASLWR Facility Mechanical Drawings [2] [25]. The model includes the primary side, secondary side, ADS system, high pressure containment, heat transfer plate, and cooling pool vessel, though only the primary side and secondary side are benchmarked for this study. A nodalization diagram is included for the entire model in 5.5, and tabulated geometric values and thermodynamic initial conditions are located in Appendix A. Note also that information on the component types can be found in reference [26]. The model runs for 8000 seconds, to provide a 2000 second stabilization time for the model. The plots included in section 5.3 only plot 2000 seconds to 8000 seconds - the time frame that models SP-3.

5.2.1 Primary Loop

The primary side includes the primary side core region, where the hot leg is represented as a vertical pipe (components 110 through 117), which connects to a branch component that models the upper plenum. The upper plenum (components 300 and 301) then connects to the pressurizer (component 310) and the cold leg, which is also modeled as a vertical pipe oriented downward (components 200 through 212). It connects to the lower plenum (component 302), which in turn connects back to the core region (component 100). There are four heat structures connected to the hot leg at various points. The first is heat structure 1100 which represents the core, and is responsible for heat input into the system. The next is heat structure 1102 which models the stainless steel wall of the hot leg riser and transfers heat between the hot leg and cold leg. The secondary side connects to the primary side via heat structure 1200 which represents the helical coil steam generator. The final heat structure is 1101 which models the heat losses to the atmosphere. A final set of components for the RPV is the charging line. The

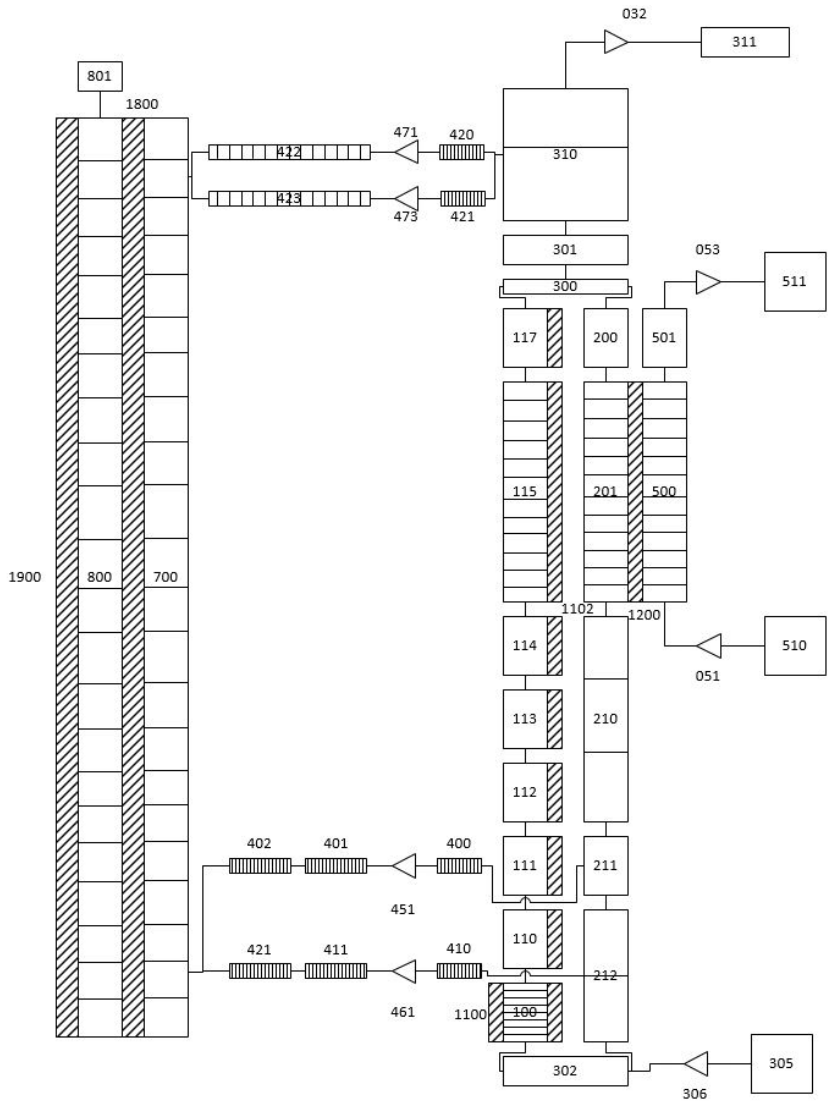

Figure 5.5: Nodalization diagram of MASLWR RELAP5-3D model

Component #	Description	DP Meter	K Factor
001	Core Exit	101	9.0
002	Chimney Exit	102	0.0
003	Reducer Exit	103	5.8
300	HLR Exit	104	17.7
014	Cold Leg Exit	106 & 106	80.0

Table 5.1: Reynold's number-independent flow loss factors

MASLWR facility features a coolant charging pump that is used to fill the RPV with cool water. This function was utilized during SP-3, so components 305 and 306 model the coolant charging pump with a time dependent volume and time dependent junction respectively.

The final table of this section (table 5.1) presents the Reynold's number-independent flow loss factors in the model. The flow losses were determined using the forced flow test, PG-1. PG-1 was also performed in 2010 and was intended to provide flow losses in the primary loop. The flow loss factors are calculated using equation (5.1) at high flow rates where the pressure losses stay roughly constant.

$$K = 2\frac{\Delta P}{\rho u^2} \tag{5.1}$$

ΔP readings are taken from DP-101 through 106 during PG-1. Recalling Figure 3.1, DP-101 measures the pressure drop across the lower plenum and the core, DP-102 measures across the chimney, DP-103 measures across the hot leg reducer, DP-104 measures across the hot leg riser, DP-105 measures across the upper plenum and steam generator, and DP-106 measures across the cold leg to the lower plenum. The DPs are positioned such that they read positive for a loss in pressure. Examination of the data from DP-105 and 106 (which share a common tap just after the steam generator) shows unexpected behavior. For the conditions over which the flow loss factors are evaluated, DP-105 remains at the top of the instrument's range with very little variation. This indicates that the pressure drop

was beyond the instrument's upper range limit. Similarly, the negative value shown by DP-106 is unexpected. Together, these indicate that the pressure reading at the RV-105 tap (the tap shared by both instruments) is extremely low. The most likely cause of this is an undeveloped flow effect coming from the steam generator shell side exit. Since these two DPs were giving incorrect readings, the flow loss coefficients cannot be determined. The chosen method then, was to calculate the flow loss coefficients for DP-101 through 104, then to correct the total flow losses in the model by making up the difference at the exit of the downcomer. This adjustment was based on maintaining the primary side flow rate at the same conditions over which the flow loss factors were evaluated.

5.2.2 Secondary Loop

The secondary side is composed of a time dependent volume (component 510) that stays at inlet conditions for the secondary side, which connects to the time dependent junction (component 051) that represents the main feed pump (MFP). The steam generator tubes are modeled as a single vertical pipe of equivalent flow area and hydraulic diameter (component 500). It connects to a valve component that is intended to allow for more complicated simulations of the secondary side (component 053). For this study, the valve was kept open to issue into the time dependent volume that exhibits the outlet conditions of the test (component 511). The secondary side connects to the primary side via heat structure 1200.

A vertical pipe was chosen for the steam generator to more accurately model the radial fluid distribution in the steam generator pipes. Fluid tumbles through the helical tube, and as it turns, the linear momentum causes a mixing effect, which is the primary reason that the helical tube promotes better heat transfer than a comparable straight-piped heat exchanger. When comparing horizontal to vertical two phase flows, the radial profiles for the velocity and temperature of a vertical flow are far more similar to those of a helical coil's radial velocity and temperature

profiles. Reference [27] suggests modeling the steam generator as a straight pipe with the same vertical inclination as the helical pitch. However, RELAP5-3D's modeling of horizontally stratified flow may be seen in figure 5.6, and an example of an air velocity profile in a helical tube can be seen in figure 5.7 [10]. Comparing the two figures indicates that the flow profile would be misrepresented by a horizontally oriented pipe. The vertical orientation over-predicts the pressure loss due to gravity, because it creates a vertical traverse of roughly 6.467 $[m]$ compared to the facility SG's vertical traverse of 1.00 $[m]$. This discrepancy is considered acceptable for this study because the validity of the scaling analysis, and therefore the model, does not depend upon a preserved boiling height in the steam generator.

Further, component 1200 utilizes shell side geometric boundary condition 134, which uses correlations for horizontal bundles of tubes. Recalling figure 3.5, the helical coil is arranged largely horizontally relative to the direction of primary flow. Therefor, the default natural convection correlation does not apply well to this scenario because it is based on a vertical flat plate [9]. Reference [9] states that option 134 makes improvements on the nucleate boiling, CHF, natural convection, and condensation correlations by implementing a correlation developed by Churchill-Chu for horizontal pipes. The natural convection is of paramount concern in single phase natural circulation flow conditions, and figure 5.8 shows the difference in the model output with the changing boundary condition.

5.2.3 ADS System

The Automatic Depressurization System (ADS), High Pressure Containment (HPC), Heat Transfer Plate (HTP), and Cooling Pool Vessel (CPV) were not utilized for this study, but are still included in the RELAP5-3D model. The ADS is composed of four pipes. For the majority of transient tests, a single vent line will be opened for depressurization into the HPC. After a certain liquid level buildup and pressure are reached, the other vent line and recirculation lines are opened. Bearing this

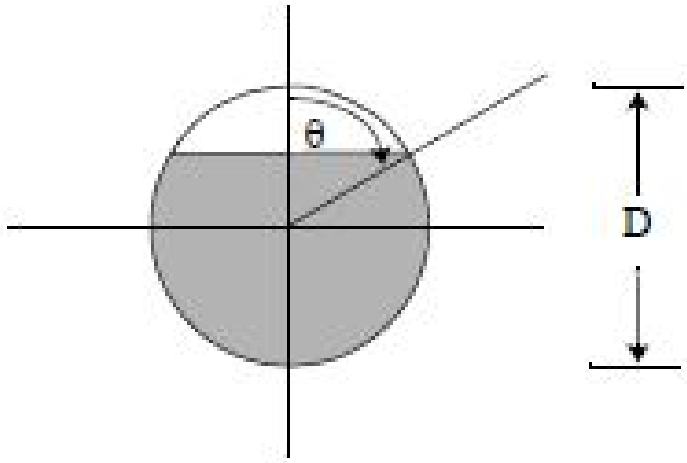

Figure 5.6: Horizontally stratified flow profile for RELAP5-3D [9]

in mind, the vent lines are split into two lines, which models the actual setup of the facility. The ADS and recirculation lines are combined into one pipe each for simplicity of modeling. Like the steam generator, the combined lines have the total cross sectional area of the two lines, and the hydraulic diameter of one line.

5.2.4 High Pressure Containment and Cooling Pool Assembly

The HPC vessel is a single pipe component (component 700) with 22 volumes. It is penetrated at two elevations by the ADS; the vent line penetration occurs at the side of volume 21, another at the entrance to volume 4 for the ADS and sump lines. The HPC pipe component increases in diameter at volume 20 to reflect the geometry of the plant. Volume 20 is sized as the average area of the expanding cone found on the HPC as a transition from the smaller diameter to the larger one.

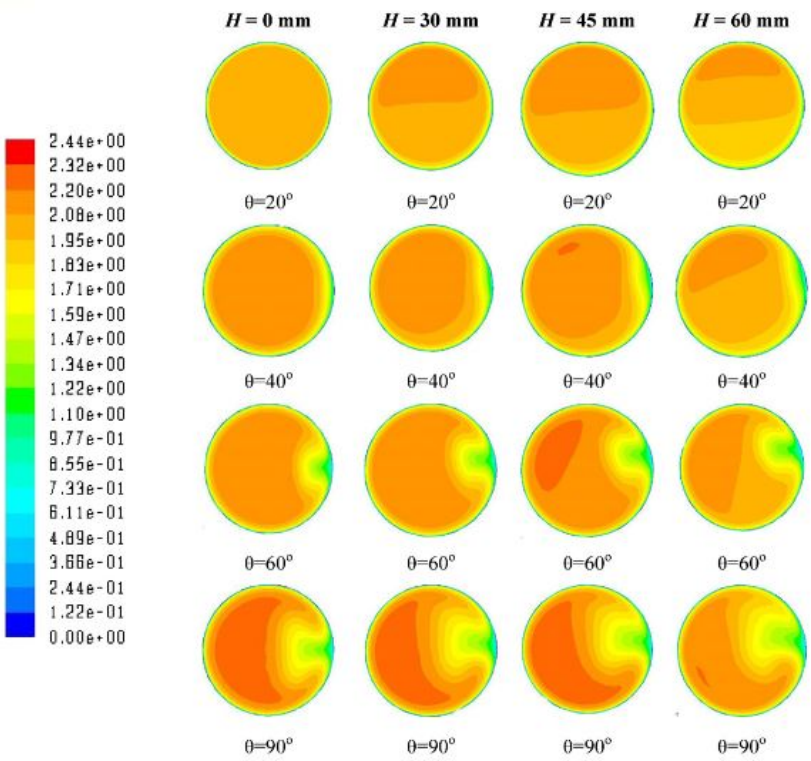

Figure 5.7: Helical coil cross sectional velocity profile for air [10]

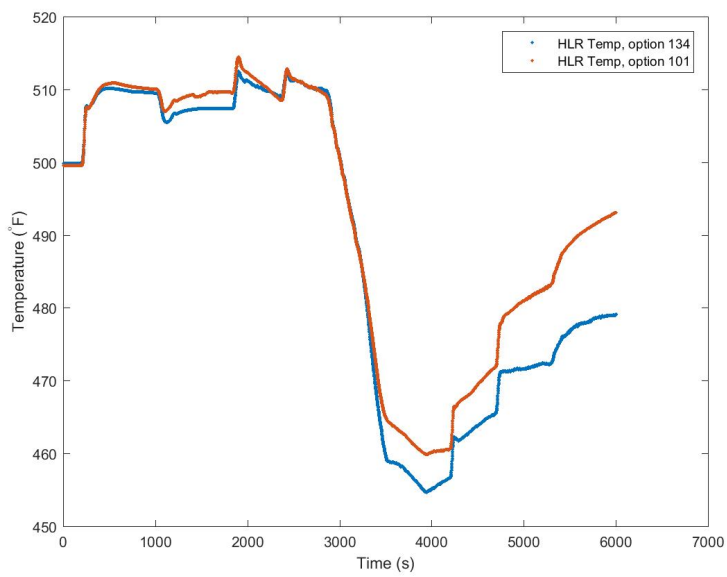

Figure 5.8: Hot leg temperatures using different geometry boundary conditions on steam generator

It is assumed that there is no heat loss from the HPC due to the fact that the HTP is intended to represent the entire heat transfer surface of the containment vessel. In order to ensure this, strip heaters are activated on the HPC on the walls around the HTP in addition to the standard insulation, to ensure that no heat can leave. Thus, there is no heat structure for ambient heat loss modeled on the HPC. The HPC wall only connects to the HTP, which is represented as heat structure 1800.

The other side of heat structure 1800 is attached to the CPV. The CPV is a single pipe component (component 800) which acts as the heat sink for the HPC. The CPV is open to atmosphere at its top, and, as such, is connected to an atmospheric time dependent volume (component 802) via a single junction (component 801). The CPV also has an ambient heat loss heat structure attached to its walls (heat structure 1900). A problem arises here because of the geometric configuration of the CPV wall. The CPV wall is made from a 10 gauge 290”$\times$93.46” steel plate that was rolled to a 30” outer diameter and originally welded to the heat transfer plate. This means that the area over which heat is lost to the environment is not a full cylinder. RELAP5-3D does not have the capability to model partial cylinders, so a cylinder with the same area as the rolled plate was used for heat structure 1900.

5.3 RELAP5-3D Results

The objective of this section is to compare the output of the RELAP5-3D model to the data of SP-3. The model was judged primarily on it’s dynamic agreement with test data, and whether or not it falls within the instrument error bars. The error bars were determined from reference [2], and were presented in figure 3.6.

5.3.1 Primary Loop Comparisons

This section presents data plots for the comparison of the RELAP5-3D model results to those of the SP-3 test data, specifically on the primary side. Imperial units are used because the facility instrument outputs are in imperial units. A full discussion of these results is presented in section 5.3.3.

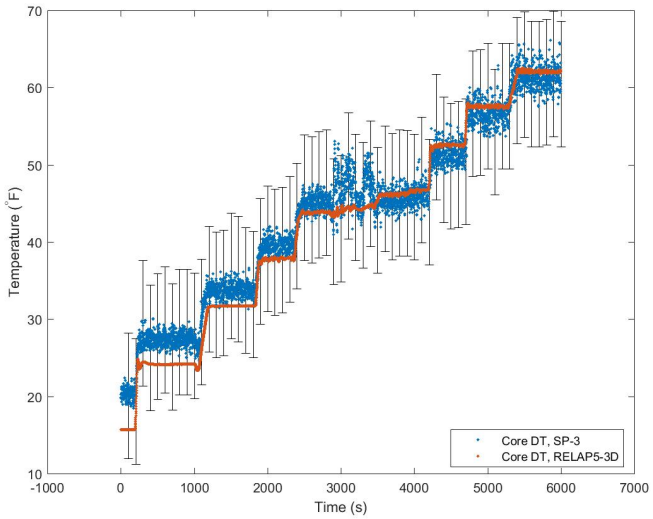

Figure 5.9: Core temperature rise comparison

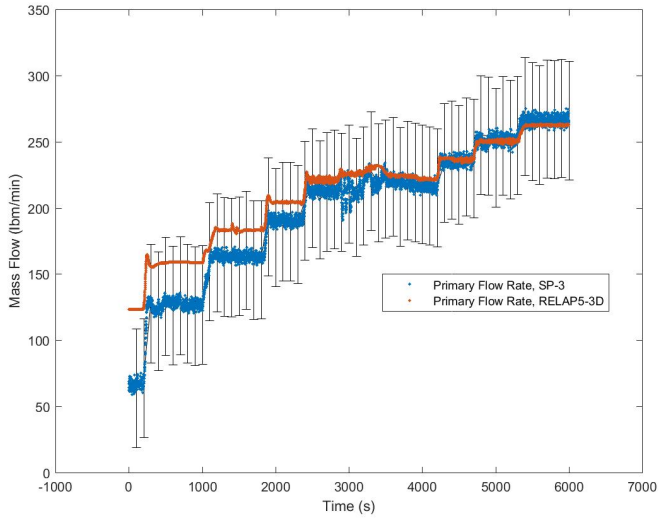

Figure 5.10: Primary side mass flow rate comparison

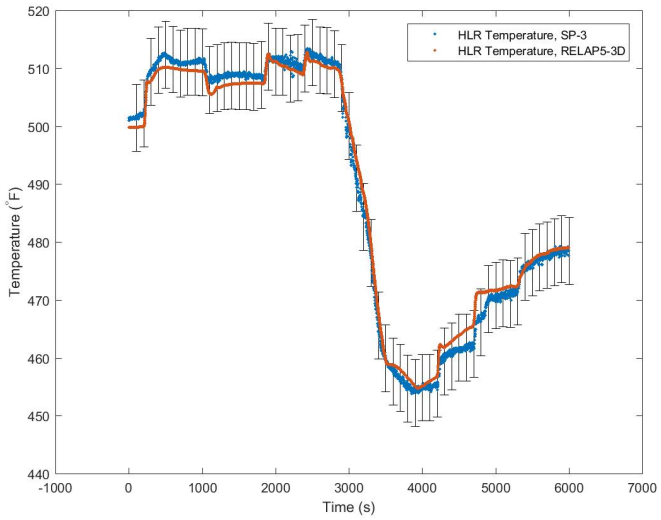

Figure 5.11: Hot leg riser temperature comparison

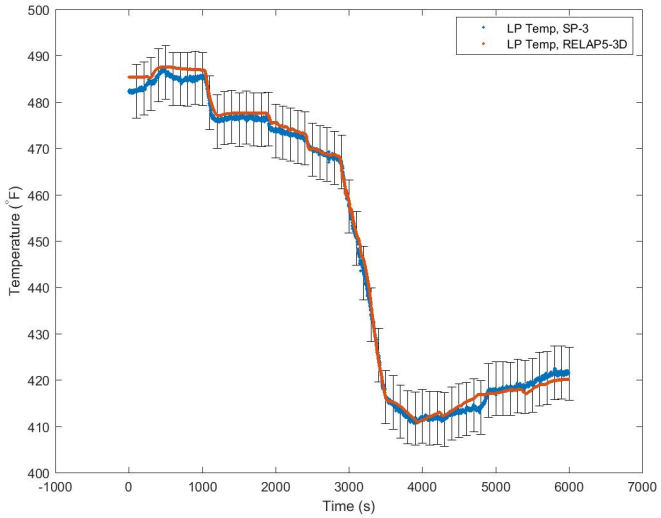

Figure 5.12: Lower plenum temperature comparison

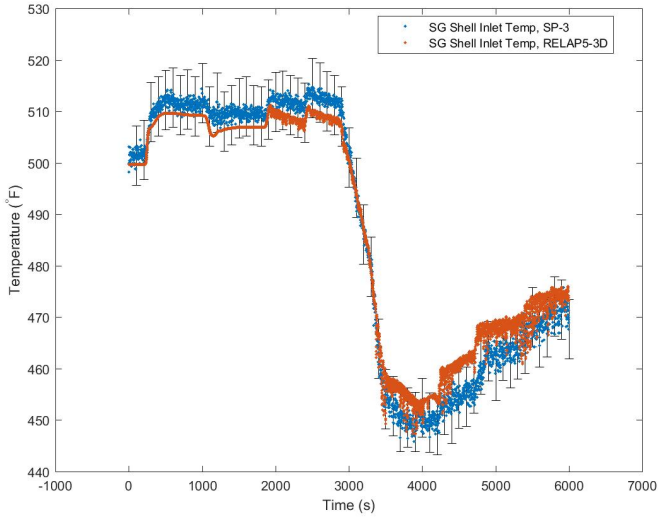

Figure 5.13: Steam generator shell side inlet temperature comparison

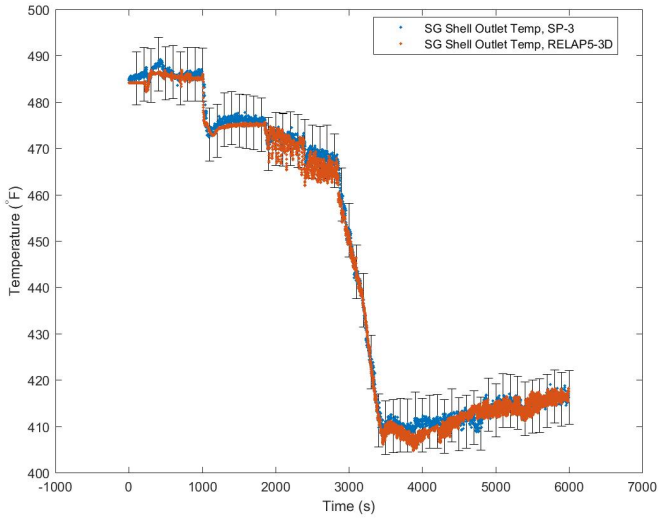

Figure 5.14: Steam generator shell side outlet temperature comparison

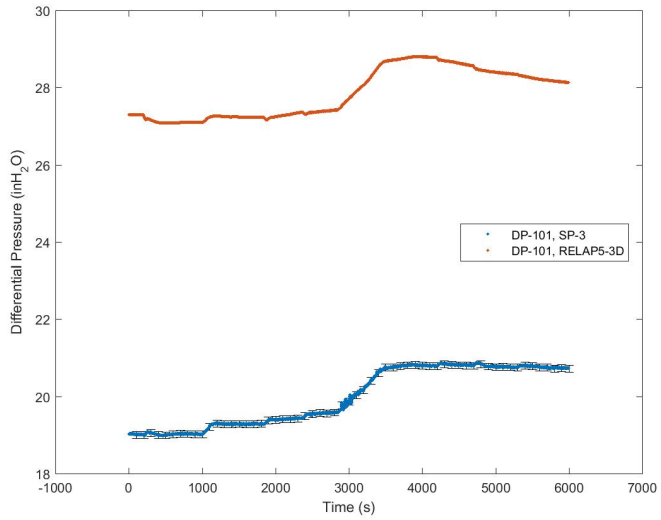

Figure 5.15: Pressure loss across core

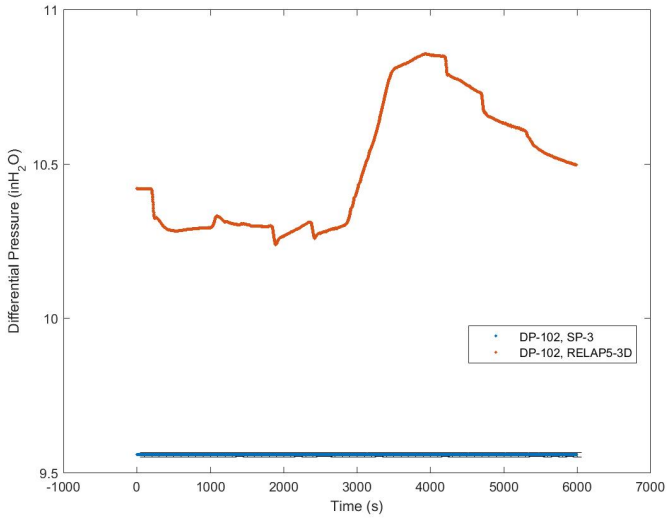

Figure 5.16: Pressure loss across chimney

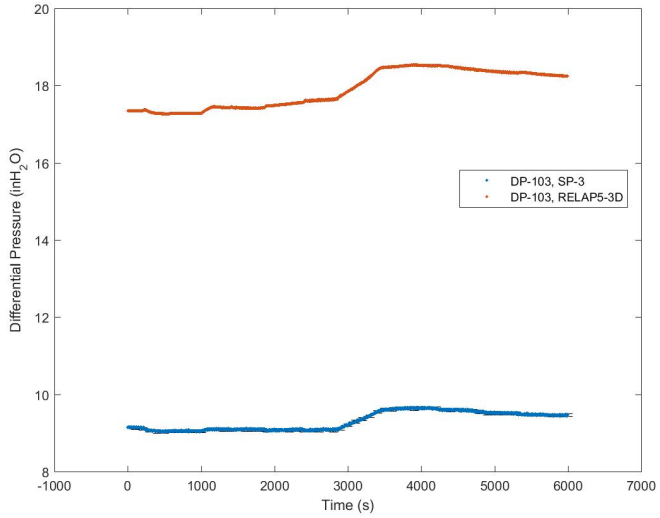

Figure 5.17: Pressure loss across hot leg reducer

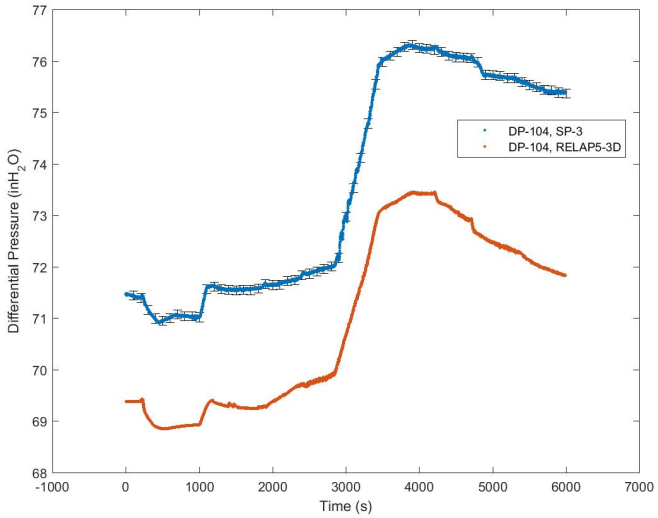

Figure 5.18: Pressure loss across hot leg riser

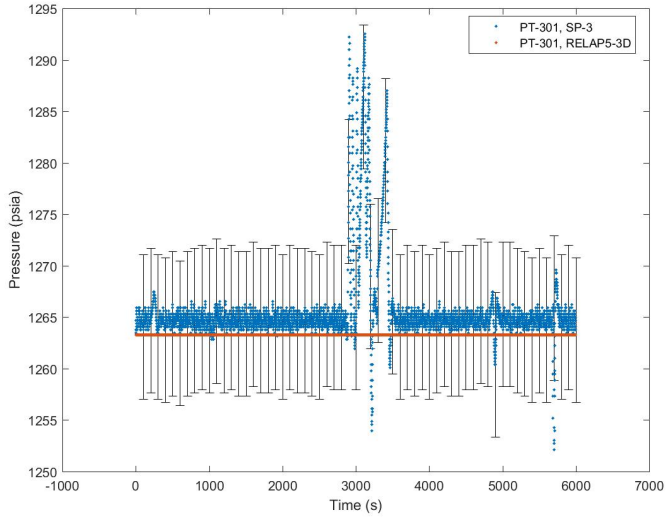

Figure 5.19: Pressurizer pressure

5.3.2 Secondary Side Comparisons

Like the previous section, this section presents data plots for the comparison of the RELAP5-3D model results to those of the SP-3 test data, specifically on the secondary side. Again, imperial units are used because of their use on the MASLWR facility.

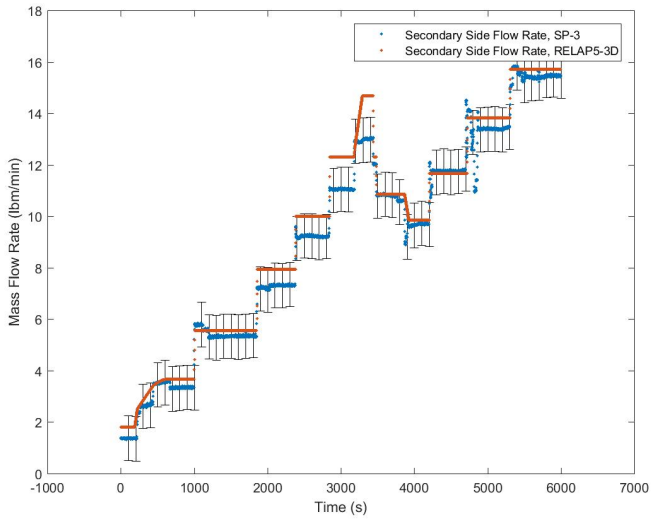

Figure 5.20: Secondary side mass flow rate comparison

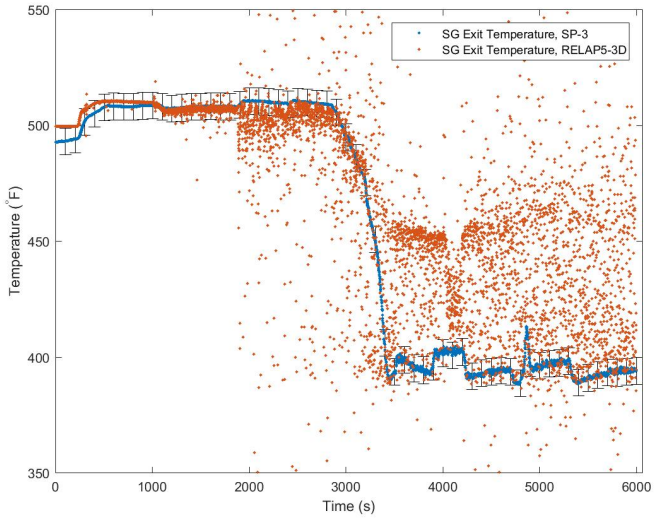

Figure 5.21: Steam generator vapor exit temperature comparison

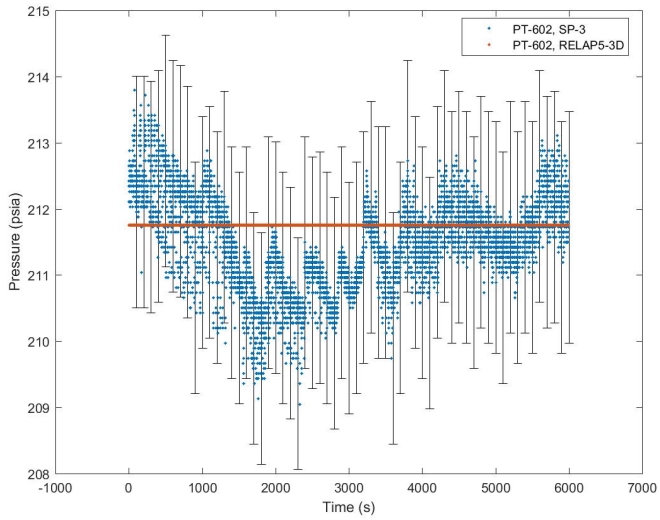

Figure 5.22: Steam generator tube side pressure

5.3.3 Discussion of Results

Figure 5.9 shows that the core temperature rise (as measured from component 302 to the exit of component 100) does not agree well at low power levels. This is also true of the primary side flow rate (Figure 5.10). In tandem, these graphs imply that the flow rate in the model is not correct, and that the RELAP model over-predicts primary side flow rates at low powers. Throughout the MASLWR program, however, FDP-131 had many problems; notably at low flow rates. Thus, a basic hand calculation (equation 5.2) was performed to determine if the flow rate measured by FDP-131 was correct.

$$\dot{Q} = \dot{m}\Delta h \tag{5.2}$$

For the measured thermodynamic conditions at 40 kW, $\Delta h = 47.7\ \frac{kJ}{kg}$, which results in a mass flow rate of $\dot{m} = 0.84\ \frac{kg}{s}$ when using equation 5.2. The facility's thermocouples were generally more reliable than the flow meter, so engineering judgement dictates that the enthalpy change be trusted over the flow meter, and thus the RELAP output for primary flow rate is trusted to be reasonably correct if this is the case. This approach however, assumes that there is no significant flow loss through the system beyond what RELAP is calculating. Thus it is possible that there are flow loss effects present in the MASLWR system that RELAP will not accurately model without further studies. Such studies were beyond the scope of this thesis, and thus, in the interest of conservatism, the RELAP model is considered to under-predict low primary system flow rates.

The hot leg riser and lower plenum temperatures agree quite well with the test data, with the exception of the two lowest power levels. The RELAP model experiences a great deal of instability at initiation, and appears to settle to temperatures that are off by roughly 2 $^{\circ}F$ in both the lower plenum (5.12) and the hot leg riser (5.11). The system temperatures agree well throughout the rest of the test.

The steam generator shell side outlet temperature agrees well with the data for the entirety of the test. The steam generator shell side inlet temperature agrees reasonably well before the large temperature transient at 3000 seconds, but is over-predicted in the latter half of the test. It is possible that the cell-centered temperature value does not match well with the thermocouple (TF-706) due to its vertical position. TF-706 is placed some distance below the true inlet (i.e. further along the steam generator) so comparison with the inlet cell in the model is incorrect. From the MASLWR documentation, the thermocouple appears to be 17.81 cm below the steam generator inlet. The closest possible cell-centered temperature is used.

Figures 5.15 through 5.18 show a good agreement in a dynamic sense, but not in a magnitude sense. This is excepting DP-102 (Figure 5.16), which appears to have been reading at its maximum value during SP-3 because the signal remains steady at one value for the duration of the test. All DPs are within the same order of magnitude from SP-3 to the RELAP model. Note that the DP test data here are presented with the reference line pressure subtracted out, giving the pressure change due to flow loss and head pressure in the flow path. This is done via the following equation, where ΔP_{true} is the pressure presented in figures 5.15 through 5.18:

$$\Delta P_{true} = P_{head} - P_{head,ref} + \Delta P_{flow} + P_{head,ref} \tag{5.3}$$

which can be written as

$$\Delta P_{true} = \Delta P_{data} + P_{head,ref} \tag{5.4}$$

Some possible reasons that the DPs don't agree well with the data are listed below:

- Cell-centered pressure values don't exactly match pressures at DP taps.
- Fluid velocities used in calculating form loss factors are determined via FDP-131 which may have had significant errors.
- DPs may be measuring undocumented flow effects, causing distorted readings.

The secondary side flow rate is within the instrument uncertainties on the vast majority of flow rates. The flow rate must be raised significantly for the flow rates between approximately 2400 and 3500 seconds. Recalling the scaling analysis of the steam generator heat transfer rate presented by equation 4.27, the heat flux is the preserved parameter. Therefore, the flow rate is not directly preserved. Based upon the scaling analysis then, the increase in flow rate is of no consequence to the validity of the model. It is also noteworthy that at the time of SP-3, NuScale Power had to increase the initial flow rate in their model to 0.015 kg/s from 0.010 kg/s shown in the test data [22]. This is comparable to the initial condition of this study, which increases initial flow to 0.0137 kg/s.

Figure 5.21 shows that the RELAP model has a very unstable temperature at the outlet of the steam generator. This is likely due to a combination of the change in thermodynamic conditions in the steam generator throughout the test, and the fact that the conditions are very close to saturation. The primary side drops in temperature, as does the steam generator. Pressure in the steam generator stays roughly constant, so the steam is not fully superheated at the exit. This is also shown by the lowest values of steam temperature lining up very well with the test data, which clearly shows saturation temperature when compared with steam table conditions. The instability is also partially due to the gradually increasing boiling height in the steam generator. Note that the model pressure is held constant at the average pressure of the secondary side because of the minor variation of the pressure.

Value	Mean Difference	Standard Deviation
Core ΔT ($^\circ F$)	2.001	1.399
Primary Flow Rate ($\frac{kg}{s}$)	0.105	0.099
Hot Leg Riser Temperature ($^\circ F$)	1.039	0.979
Lower Plenum Temperature ($^\circ F$)	1.572	0.919
SG Shell Inlet Temperature ($^\circ F$)	3.432	2.059
SG Shell Outlet Temperature ($^\circ F$)	1.532	1.246
Core Pressure Loss (inH_2O)	7.856	0.206
Core Outlet Pressure Loss (inH_2O)	0.931	0.207
Reducer Pressure Loss (inH_2O)	8.597	0.258
Hot Leg Riser Pressure Loss (inH_2O)	2.616	0.497
Primary Pressure (psi)	2.428	3.927
Secondary Flow Rate ($\frac{kg}{s}$)	0.0035	0.0033
Average SG Exit Temperature ($^\circ F$)	24.719	31.557
Secondary Pressure (psi)	0.606	0.446

Table 5.2: Mean differences between RELAP output and test data, and their standard deviations

Chapter 6: Conclusions and Future Work

This chapter offers summarizing statements on the work presented herein, and also proposes possible future work ideas, should the study require improvement.

6.1 Conclusions

This study set out to develop a RELAP5-3D model for use in load following studies, and to define a new set of scaling parameters for the OSU MASLWR system. The updated scaling was required because the MASLWR system was not originally scaled to full-power operations which is necessary for Idaho National Laboratory's studies using the RELAP5-3D model. The new set of scaling parameters developed in chapter 4 gives reasonable values for the single phase solution, but cannot be extended to two-phase conditions because of a lack of information on the NuScale core. In this regard, the new analysis is useful, but limited in its applications. The old and new MASLWR scaling parameters are summarized in table 6.1 for the reader's convenience.

Scaling Ratio	Original Scaling Factor	New Scaling Factor
L_R	$\frac{1}{3.1}$	$\frac{1}{3.1}$
$L_{SG,R}$	$\frac{1}{3.1}$	$\frac{1}{3.1}$
A_R	$\frac{1}{82.2}$	$\frac{1}{82.2}$
$A_{SG,R}$	$\frac{1}{254.7}$	$\frac{1}{254.7}$
V_R	$\frac{1}{254.7}$	$\frac{1}{254.7}$
$\left(\frac{A_c}{A_i}\right)_R$	1	1
$\Pi_{F,R}$	3.1	3.1
$Prop_R$	1	1
$\Pi_{SG,R}$	1	1
τ_R	1	1.14
$q_{core,R}$	$\frac{1}{254.7}$	$\frac{1}{376.39}$
u_R	$\frac{1}{3.1}$	$\frac{1}{3.53}$
$\Delta T_{core,R}$	1	$\frac{1}{1.30}$
$(U_{SG}\Delta T_{SG})_R$	1	$\frac{1}{1.48}$

Table 6.1: Original MASLWR scaling ratios

The RELAP5-3D model is considered to adequately model the MASLWR system. The thermodynamic quantities presented herein agree well with test data. Flow loss and flow rate quantities do not agree well without adjustments to the model, i.e. tuning the flow losses where they could not be calculated due to poor instrumentation. Because this approach was taken, the precise flow losses of the model that are presented in figures 5.15 through 5.18 are of little consequence to the total loop flow losses, and are thus not a concern. However, in conjunction with the discussion of section 5.3.3 regarding primary loop flow losses, the total loop flow losses are not predicted well at low flow rates.

6.2 Future Work

Recalling the contents of section 1.3, it is intended that this model and accompanying scaling analysis will be utilized by Idaho National Laboratory to aid in simulations of hybrid energy systems, which is intended to be the majority of the future work for this study. It may be useful, however, to improve on this study in the following ways. A two-phase scaling analysis would be very useful from the standpoint of what kind of simulations can be run with this model. Recalling the discussion in section 4.2, the MASLWR system can experience subcooled boiling under the proper conditions. In order for the study to be more encompassing, a two-phase scaling analysis should be performed if the proper information can be obtained from NuScale Power. Further, the flow losses should be improved if possible. Although the flow losses for this study are deemed sufficient, they could be improved if better data on MASLWR could be obtained. Due to the MASLWR's decommissioning, this is unlikely; however, it cannot be ruled out at this time. Finally, the MASLWR no longer accurately represents the NuScale Power SMR design. Significant design changes are what finally pushed NuScale Power to replace the MASLWR facility in 2014. If data could be used for the NIST-1 facility (the MASLWR's successor, whose data is, at this time, largely proprietary) for this same purpose, it would service a more contemporary design. This would ensure better applicability of the hybrid energy research being performed at INL.

Bibliography

[1] et al. Shannon M. Bragg-Sitton. Nuclear-renewable hybrid energy systems: 2016 technology development program plan. *Idaho National Laboratory and Oak Ridge National Laboratory*, 2016.

[2] John T. Groome Brian G. Woods Nathan T. Demick, Mark R. Galvin. OSU-MASLWR test facility description report. *Department of Nuclear Engineering and Radition Health Physics, Oregon State University*, 2007.

[3] Charles Forsberg. Hybrid systems to addres seasonal mismatches between electricity production and demand in nuclear renewable energy grids. *Energy Policy*, pages 333–341, 2013.

[4] et al. Humberto E. Garcia. Nuclear hybrid energy systems - regional studies: West texas and northeastern arizona. *Idaho National Laboratory*, 2015.

[5] N. Zuber et al. An integrated structure and scaling methodolgy for severe accident technical issue resolution: Development of methodology. *Nuclear Engineering and Design*, 186:1–21, 1998.

[6] Lawrence Hochreiter Jose N. Reyes Jr. Scaling analysis for the OSU AP600 test facility (APEX). *Nuclear Engineering and Design*, 186:53–109, 1998.

[7] et al. Brian G. Woods. Analyses of the OSU-MASLWR experimental test facility. *Science and Technology of Nuclear Installations*, 2012, 2012.

[8] John King Jose N. Reyes, Jr. Scaling analysis for the OSU integral system test facility. *Department of Nuclear Engineering, Oregon State University*, pages 1–38, 2003.

[9] Idaho National Engineering Laboratory. *RELAP5-3D Code Manual Volume IV: Models and Correlations*, 2012.

[10] J.C. Mandal Kannan N. Iyer P.K. Vijayan J.S. Jayakumar, S.M. Mahajani. Thermal hydraulic characteristics of air-water two-phase flows in helical pipes. *Chemical Engineering Research and Design*, pages 501–512, 2009.

[11] L.S. Khrilev I.A. Smirnov, K.S. Svetlov. Selecting main technical solutions for heat supply systems equipped with nuclear cogeneration stations. *Thermal Engineering*, 55:939–946, 2008.

[12] et al. Shannon M. Bragg-Sitton. Integrated nuclear-renewable energy systems: Foundational workshop report. *Idaho National Laboratory, National Renewable Energy Laboratory, Massachusetts Institute of Technology*, 2014.

[13] et al. Man Gyun Na. A model predictive controller for load-following operation of PWR reactors. *IEEE Transactions on Nuclear Science*, 52:1009–1020, 2005.

[14] et al. Sim Won Lee. Design of a load following controller for APR+ nuclear plants. *Department of Nuclear Engineering, Chosun University*, 2012.

[15] A. Lokhov. Load-following with nuclear power plants. *NEA Updates, NEA News*, 29.2:18–20, 2011.

[16] J. Burns. Applied control strategies at a cogeneration plant. 2011.

[17] Charles Forsberg. Future hydrogen markets for large-scale hydrogen production systems. *International Journal of Hydrogen Energy*, pages 431–439, 2006.

[18] Idaho National Engineering Laboratory. *RELAP5-3D Code Manual Volume I: Code Structure, System Models and Solution Methods*, 2012.

[19] M. Colombo et al. Thermal hydraulic characteristics of air-water two-phase flows in helical pipes. *Progress in Nuclear Energy*, pages 15–23, 2012.

[20] L. Winters. NUREG/IA-0091, assessment of RELAP5/MOD2 against a natural circulation experiment in nuclear power plant borssele. 1993.

[21] A. Mangal et al. Capability of the RELAP5 code to simulate natural circulation behavior in test facilities. *Progress in Nuclear Energy*, 61:1–16, 2012.

[22] International Atomic Energy Agency. IAEA-TECDOC-1733: Evaluation of advanced thermohydraulic system codes for design and safety analysis of integral type reactors. *International Atomic Energy Agency*, pages 27–31, 2014.

[23] Mujid S. Kazimi Neil E. Todreas. *Nuclear Systems Volume I: Thermal Hydraulic Fundamentals*. CRC Press, Taylor & Francis Group, 6000 Broken Sound Parkway NW, Suite 300, Boca Raton, FL, 33487-2742, 2012.

[24] Hu Luo Anh T. Mai. OSU-MASLWR test facility quick look report. *OSU-MASLWR-QLR-SP3 (Rev 0)*, 2011.

[25] Oregon State University. *OSU MASLWR Facility Mechanical Drawings*, 2014.

[26] Idaho National Engineering Laboratory. *Appendix A: RELAP5-3D Input Data Requirements*, 2012.

[27] Nolan A. Anderson Nathan V. Hoffer, Piyush Sabharwall. Modeling a helical-coil steam generator in RELAP5-3D for the next generation nuclear plant. *Idaho National Laboratory*, 2011.

APPENDICES

Appendix A: RELAP5-3D Tabulated Parameters

This appendix contains tabulated values of the RELAP5-3D model developed for this study.

A.1 Geometric Values

Component #	Cell #	Type	Flow Area (m^2)	D_H (m)	Length (m)
100	1	Pipe	$8.42E-3$	$9.59E-3$	$7.75E-2$
	2	Pipe	$8.42E-3$	$9.59E-3$	$7.75E-2$
	3	Pipe	$8.42E-3$	$9.59E-3$	$7.75E-2$
	4	Pipe	$8.42E-3$	$9.59E-3$	$7.75E-2$
	5	Pipe	$8.42E-3$	$9.59E-3$	$7.75E-2$
	6	Pipe	$8.42E-3$	$9.59E-3$	$7.75E-2$
	7	Pipe	$8.42E-3$	$9.59E-3$	$7.75E-2$
	8	Pipe	$8.42E-3$	$9.59E-3$	$7.75E-2$
001	N/A	Sngljun	$3.05E-2$	$1.97E-1$	N/A
110	1	Snglvol	$3.05E-2$	$1.94E-1$	$4.3E-1$
002	N/A	Sngljun	$3.05E-2$	$1.97E-1$	N/A
111	1	Snglvol	$1.88E-2$	$1.53E-1$	$2.4E-1$
003	N/A	Sngljun	$8.21E-3$	$1.03E-1$	N/A
112	1	Snglvol	$8.21E-3$	$1.03E-1$	$8.6E-1$
004	N/A	Sngljun	$8.21E-3$	$1.03E-1$	N/A
113	1	Snglvol	$6.57E-3$	$5.26E-2$	$1.1E-1$
005	N/A	Sngljun	$6.57E-3$	$9.15E-2$	N/A
114	1	Snglvol	$8.21E-3$	$1.03E-1$	$5.0E-2$

Table A.1: RPV Geometric Parameters (continued on next page)

Component #	Cell #	Type	Flow Area (m^2)	D_H (m)	Length (m)
006	N/A	Sngljun	$8.21E-3$	$1.03E-1$	N/A
115	1	Pipe	$8.21E-3$	$1.03E-1$	$2.30E-2$
	2	Pipe	$8.21E-3$	$1.03E-1$	$2.30E-2$
	3	Pipe	$8.21E-3$	$1.03E-1$	$2.30E-2$
	4	Pipe	$8.21E-3$	$1.03E-1$	$2.30E-2$
	5	Pipe	$8.21E-3$	$1.03E-1$	$1.02E-1$
	6	Pipe	$8.21E-3$	$1.03E-1$	$1.02E-1$
	7	Pipe	$8.21E-3$	$1.03E-1$	$1.02E-1$
	8	Pipe	$8.21E-3$	$1.03E-1$	$1.02E-1$
	9	Pipe	$8.21E-3$	$1.03E-1$	$1.02E-1$
	10	Pipe	$8.21E-3$	$1.03E-1$	$1.02E-1$
	11	Pipe	$8.21E-3$	$1.03E-1$	$1.02E-1$
	12	Pipe	$8.21E-3$	$1.03E-1$	$7.62E-2$
008	N/A	Sngljun	$8.21E-3$	$1.03E-1$	N/A
117	1	Snglvol	$8.21E-3$	$1.03E-1$	$2.0E-1$
300	N/A	Branch	$6.7E-2$	$2.92E-1$	$7.00E-2$
301	N/A	Snglvol	$6.7E-2$	$2.92E-1$	$1.50E-1$
031	N/A	Sngljun	$6.7E-2$	$2.92E-1$	N/A
310	1	Pipe	$6.7E-2$	$2.92E-1$	$3.6E-1$
	2	Pipe	$6.7E-2$	$2.92E-1$	$3.0E-1$
311	N/A	Tmdpvol	1.0	1.128	1.0
032	N/A	Valve	$6.7E-2$	$2.92E-1$	N/A
009	N/A	Sngljun	$6.7E-2$	$2.92E-1$	N/A
200	1	Snglvol	$5.68E-2$	$1.78E-1$	$2.0E-1$
010	N/A	Sngljun	$5.11E-2$	$2.55E-1$	N/A

Table A.1: RPV Geometric Parameters (continued on next page)

Component #	Cell #	Type	Flow Area (m^2)	D_H (m)	Length (m)
201	1	Pipe	$5.1E-2$	$7.55E-2$	$7.60E-2$
	2	Pipe	$3.69E-2$	$2.36E-2$	$1.16E-1$
	3	Pipe	$3.69E-2$	$2.36E-2$	$1.16E-1$
	4	Pipe	$3.69E-2$	$2.36E-2$	$1.16E-1$
	5	Pipe	$3.69E-2$	$2.36E-2$	$1.16E-1$
	6	Pipe	$3.69E-2$	$2.36E-2$	$1.16E-1$
	7	Pipe	$3.69E-2$	$2.36E-2$	$1.16E-1$
	8	Pipe	$3.69E-2$	$2.36E-2$	$1.16E-1$
	9	Pipe	$3.69E-2$	$2.36E-2$	$2.30E-2$
	10	Pipe	$3.69E-2$	$2.36E-2$	$2.30E-2$
	11	Pipe	$3.69E-2$	$2.36E-2$	$2.30E-2$
	12	Pipe	$3.69E-2$	$8.47E-2$	$2.30E-2$
011	N/A	Sngljun	$3.69E-2$	$8.47E-2$	N/A
210	1	Pipe	$5.68E-2$	$1.78E-1$	$5.0E-2$
	2	Pipe	$5.68E-2$	$1.78E-1$	$1.1E-1$
	3	Pipe	$5.68E-2$	$1.78E-1$	$1.1E-1$
012	N/A	Sngljun	$5.68E-2$	$1.78E-1$	N/A
211	N/A	Branch	$4.67E-2$	$1.32E-1$	2.4E-1
013	N/A	Sngljun	$4.67E-2$	$1.32E-1$	N/A
212	1	Pipe	$3.46E-2$	$8.9E-2$	$4.3E-1$
	2	Pipe	$3.46E-2$	$8.9E-2$	$6.2E-1$
014	N/A	Sngljun	$3.46E-2$	$8.9E-2$	N/A
302	N/A	Branch	$6.7E-2$	$2.92E-1$	7.0E-2
015	N/A	Sngljun	$6.7E-2$	$2.92E-1$	N/A
305	1	Tmdpvol	$1.27E-4$	$1.27E-2$	1.0
306	N/A	Tmdpjun	$1.27E-4$	$1.27E-2$	N/A

Table A.1: RPV Geometric Parameters

Shown below is the table of geometric values for the secondary side.

Component #	Cell #	Type	Flow Area (m^2)	D_H (m)	Length (m)
510	1	Tmdpvol	$1.74E-3$	$4.70E-2$	1.0
051	N/A	Tmdpjun	$1.74E-3$	$4.70E-2$	N/A
500	1	Pipe	$1.63E-3$	$1.26E-2$	$1.24E-1$
	2	Pipe	$1.63E-3$	$1.26E-2$	$1.24E-1$
	3	Pipe	$1.63E-3$	$1.26E-2$	$1.24E-1$
	4	Pipe	$1.63E-3$	$1.26E-2$	$1.24E-1$
	5	Pipe	$1.63E-3$	$1.26E-2$	$7.95E-1$
	6	Pipe	$1.63E-3$	$1.26E-2$	$7.95E-1$
	7	Pipe	$1.63E-3$	$1.26E-2$	$7.95E-1$
	8	Pipe	$1.63E-3$	$1.26E-2$	$7.95E-1$
	9	Pipe	$1.63E-3$	$1.26E-2$	$7.95E-1$
	10	Pipe	$1.63E-3$	$1.26E-2$	$7.95E-1$
	11	Pipe	$1.63E-3$	$1.26E-2$	$7.95E-1$
	12	Pipe	$1.63E-3$	$1.26E-2$	$4.09E-2$
052	N/A	Sngljun	$1.63E-3$	$1.26E-2$	N/A
501	1	Snglvol	$1.0E-2$	$1.13E-2$	$3.0E-1$
053	N/A	Valve	$2.5E-4$	$1.78E-2$	N/A
511	1	Tmdpvol	$1.0E-2$	$1.13E-1$	1.0

Table A.2: Secondary Side Geometric Parameters

A.2 Thermodynamic Initial Conditions

The thermodynamic initial conditions of the primary side are presented in A.3:

Component #	Cell #	Type	Pressure (Pa)	Temp (K)	Flow Rate ($\frac{kg}{s}$)
100	1	Pipe	$8.71E6$	525.2	$8.7E-1$
	2	Pipe	$8.71E6$	526.3	$8.7E-1$
	3	Pipe	$8.71E6$	527.4	$8.7E-1$
	4	Pipe	$8.71E6$	528.5	$8.7E-1$
	5	Pipe	$8.71E6$	529.7	$8.7E-1$
	6	Pipe	$8.71E6$	530.8	$8.7E-1$
	7	Pipe	$8.71E6$	533.9	$8.7E-1$
	8	Pipe	$8.71E6$	535.0	N/A
001	N/A	Sngljun	N/A	N/A	$8.7E-1$
110	1	Snglvol	$8.71E6$	535.0	N/A
002	N/A	Sngljun	N/A	N/A	$8.7E-1$
111	1	Snglvol	$8.71E6$	535.0	N/A
003	N/A	Sngljun	N/A	N/A	$8.7E-1$
112	1	Snglvol	$8.71E6$	535.0	N/A
004	N/A	Sngljun	N/A	N/A	$8.7E-1$
113	1	Snglvol	$8.71E6$	535.0	N/A
005	N/A	Sngljun	N/A	N/A	$8.7E-1$
114	1	Snglvol	$8.71E6$	535.0	N/A
006	N/A	Sngljun	N/A	N/A	$8.7E-1$

Table A.3: RPV Thermodynamic Conditions (continued on next page)

Component #	Cell #	Type	Pressure (Pa)	Temp (K)	Flow Rate ($\frac{kg}{s}$)
115	1	Pipe	$8.71E6$	535.0	$8.7E-1$
	2	Pipe	$8.71E6$	535.0	$8.7E-1$
	3	Pipe	$8.71E6$	535.0	$8.7E-1$
	4	Pipe	$8.71E6$	535.0	$8.7E-1$
	5	Pipe	$8.71E6$	535.0	$8.7E-1$
	6	Pipe	$8.71E6$	535.0	$8.7E-1$
	7	Pipe	$8.71E6$	535.0	$8.7E-1$
	8	Pipe	$8.71E6$	535.0	$8.7E-1$
	9	Pipe	$8.71E6$	535.0	$8.7E-1$
	10	Pipe	$8.71E6$	535.0	$8.7E-1$
	11	Pipe	$8.71E6$	535.0	$8.7E-1$
	12	Pipe	$8.71E6$	535.0	N/A
008	N/A	Sngljun	N/A	N/A	$8.7E-1$
117	1	Snglvol	$8.71E6$	535.0	N/A
300	N/A	Branch	$8.71E6$	535.0	$8.7E-1$
301	N/A	Snglvol	$8.71E6$	535.0	N/A
031	N/A	Sngljun	N/A	N/A	0.0
310	1	Pipe	$8.71E6$	Sat ($x = 0.027$)	0.0
	2	Pipe	$8.71E6$	Sat ($x = 1.0$)	0.0
311	N/A	Tmdpvol	$8.71E6$	Sat ($x = 1.0$)	N/A
032	N/A	Valve	N/A	N/A	0.0
009	N/A	Sngljun	N/A	N/A	$8.7E-1$
200	1	Snglvol	$8.71E6$	535.0	N/A
010	N/A	Sngljun	N/A	N/A	$8.7E-1$

Table A.3: RPV Thermodynamic Conditions (continued on next page)

Component #	Cell #	Type	Pressure (Pa)	Temp (K)	Flow Rate ($\frac{kg}{s}$)
201	1	Pipe	$8.71E6$	535.0	$8.7E-1$
	2	Pipe	$8.71E6$	534.0	$8.7E-1$
	3	Pipe	$8.71E6$	533.0	$8.7E-1$
	4	Pipe	$8.71E6$	532.0	$8.7E-1$
	5	Pipe	$8.71E6$	531.0	$8.7E-1$
	6	Pipe	$8.71E6$	530.0	$8.7E-1$
	7	Pipe	$8.71E6$	529.0	$8.7E-1$
	8	Pipe	$8.71E6$	528.0	$8.7E-1$
	9	Pipe	$8.71E6$	524.0	$8.7E-1$
	10	Pipe	$8.71E6$	524.0	$8.7E-1$
	11	Pipe	$8.71E6$	524.0	$8.7E-1$
	12	Pipe	$8.71E6$	524.0	N/A
011	N/A	Sngljun	N/A	N/A	$8.7E-1$
210	1	Pipe	$8.71E6$	528.2	$8.7E-1$
	2	Pipe	$8.71E6$	528.2	$8.7E-1$
	3	Pipe	$8.71E6$	528.2	N/A
012	N/A	Sngljun	N/A	N/A	$8.7E-1$
211	N/A	Branch	$8.71E6$	527.2	N/A
013	N/A	Sngljun	N/A	N/A	$8.7E-1$
212	1	Pipe	$8.71E6$	526.2	$8.7E-1$
	2	Pipe	$8.71E6$	526.2	N/A
014	N/A	Sngljun	N/A	N/A	$8.7E-1$
302	N/A	Branch	$8.71E6$	525.2	N/A
015	N/A	Sngljun	N/A	N/A	$8.7E-1$
305	1	Tmdpvol	$8.71E6$	293.0	N/A
306	N/A	Tmdpjun	N/A	N/A	0.0

Table A.3: RPV Thermodynamic Conditions

The charging pump was activated during the test. Component 306 represents the coolant charging pump. This pump changes flow rate throughout the test, so its flow rates are tabulated in table A.4 below.

Time (s)	Liquid Flow Rate ($\frac{kg}{s}$)	Vapor Flow Rate ($\frac{kg}{s}$)
0.0	0.0	0.0
4896.0	0.0	0.0
4909.0	$8.2E-3$	0.0
4916.0	0.0	0.0
4944.0	0.0	0.0
4950.0	$7.3E-3$	0.0
4956.0	$8.2E-3$	0.0
4960.0	0.0	0.0
5007.0	0.0	0.0
5017.0	$8.5E-3$	0.0
5021.0	0.0	0.0
5044.0	0.0	0.0
5051.0	$3.3E-3$	0.0
5124.0	$3.3E-3$	0.0
5126.0	0.0	0.0
5153.0	0.0	0.0
5157.0	$3.3E-3$	0.0
5180.0	$3.5E-3$	0.0
5181.0	0.0	0.0
5300.0	0.0	0.0
5304.0	$3.3E-3$	0.0
5428.0	$3.3E-3$	0.0
5430.0	0.0	0.0

Table A.4: Coolant Charging Pump Flow Rates

Table A.5 shows the thermodynamic values for the secondary side.

Component #	Cell #	Type	Pressure (Pa)	Temp (K)	Flow Rate ($\frac{kg}{s}$)
510	1	Tmdpvol	$1.46E6$	293.0	N/A
051	N/A	Tmdpjun	N/A	N/A	$1.37E-2$
500	1	Pipe	$1.46E6$	310.8	$1.0E-2$
	2	Pipe	$1.46E6$	315.0	$1.0E-2$
	3	Pipe	$1.46E6$	320.0	$1.0E-2$
	4	Pipe	$1.46E6$	330.0	$1.0E-2$
	5	Pipe	$1.46E6$	333.2	$1.0E-2$
	6	Pipe	$1.46E6$	352.0	$1.0E-2$
	7	Pipe	$1.46E6$	365.6	$1.0E-2$
	8	Pipe	$1.46E6$	398.0	$1.0E-2$
	9	Pipe	$1.46E6$	430.4	$1.0E-2$
	10	Pipe	$1.46E6$	462.8	$1.0E-2$
	11	Pipe	$1.46E6$	495.2	$1.0E-2$
	12	Pipe	$1.46E6$	527.6	N/A
052	N/A	Sngljun	N/A	N/A	$1.0E-2$
501	1	Snglvol	$1.46E6$	482.0	N/A
053	N/A	Valve	N/A	N/A	$1.0E-2$
511	1	Tmdpvol	$1.46E6$	508.7	N/A

Table A.5: Secondary Side Thermodynamic Conditions

Component 051 is a time dependent junction that represents the main feed pump by providing feedwater flow. It changes throughout the test to match the flow rates in SP-3. Its values are tabulated below in table A.6.

Time (s)	Liquid Flow Rate ($\frac{kg}{s}$)	Vapor Flow Rate ($\frac{kg}{s}$)
0.0	$1.37E-2$	0.0
2190.0	$1.37E-2$	0.0
2225.0	$2.02E-2$	0.0
2446.0	$2.66E-2$	0.0
2582.0	$2.76E-2$	0.0
2673.0	$2.77E-2$	0.0
3001.0	$2.77E-2$	0.0
3006.0	$4.20E-2$	0.0
3853.0	$4.20E-2$	0.0
3858.0	$6.00E-2$	0.0
4380.0	$6.00E-2$	0.0
4384.0	$7.55E-2$	0.0
4844.0	$7.55E-2$	0.0
4847.0	$9.30E-2$	0.0
5184.0	$9.30E-2$	0.0
5189.0	$9.55E-2$	0.0
5293.0	$1.11E-1$	0.0
5442.0	$1.11E-1$	0.0
5446.0	$9.30E-2$	0.0
5485.0	$9.30E-2$	0.0
5489.0	$8.10E-2$	0.0
5870.0	$8.10E-2$	0.0
5926.0	$7.35E-2$	0.0
6204.0	$7.35E-2$	0.0

Table A.6: Main Feed Pump Flow Rates (continued on next page)

Time (s)	Liquid Flow Rate ($\frac{kg}{s}$)	Vapor Flow Rate ($\frac{kg}{s}$)
6209.0	$8.82E-2$	0.0
6719.0	$8.82E-2$	0.0
6724.0	$1.045E-1$	0.0
7306.0	$1.045E-1$	0.0
7311.0	$1.187E-1$	0.0
7312.0	$1.187E-1$	0.0

Table A.6: Main Feed Pump Flow Rates